Zero-Temperature DWF Physics from QCDOC

Saul D. Cohen

sdcohen@phys.columbia.edu

for the RBC and UKQCD Collaborations

(Columbia University)

Outline

Lattice Generation

– Action selection
– Algorithm improvement
– Parameter tuning

Lattice Properties

– Run progress
– Spectrum and residual mass
– Decay constant and scale setting

Lattice Calculations

– Kaon bag parameter
– Chiral fitting
– Convolved source

Lattice Generation

Action Selection

The action must compromise between desire for good chiral symmetry, fine lattice spacing and fast topology change.

Algorithm Improvement

Rational HMC, quotient HMC and Omelyan integrator make implementation possible.

Parameter Tuning

Tuning adjustable parameters in the algorithm improves acceptance rate, increasing production speed.

Action Selection

Chiral Symmetry

Chiral symmetry is important to a number of activities, such as weak matrix elements. Particularly important to B_K to suppress mixing with wrong-chirality operators.

Domain-Wall Fermions

The RBC group has extensive experience with the DWF formalism, which provides systematic control over chiral symmetry breaking by adjustment of the fifth dimensional size.

Residual Mass

We parametrize the amount of chiral symmetry breaking by the residual mass. Making the residual mass significantly smaller than our lightest quark mass is a priority.

Action Improvement

Rectangle Term

By smoothing the gauge fields, a smaller residual mass may be obtained. A rectangle term smooths the gauge fields at short range while having no impact in the continuum limit.

Rectangle Parameter Space

Our action is parametrized as

$$S_g = -\frac{\beta}{3}\sum_x \left((1-8c_1)\,\mathrm{Tr}\,U_{\mathrm{plaq}} + c_1 \mathrm{Tr}\,U_{\mathrm{rect}}\right)$$

forming a 2-parameter space of $\{\beta, c_1\}$. The Wilson, DBW2 and Iwasaki actions are lines of constant c_1 in this space. By increasing c_1 while decreasing β, we may reduce the residual mass and keep the lattice scale fixed.

Action Improvement

Exploration of Rectangle Space

An exploration of the rectangle space was conducted on small $16^3 \times 32$ 3-flavor lattices.

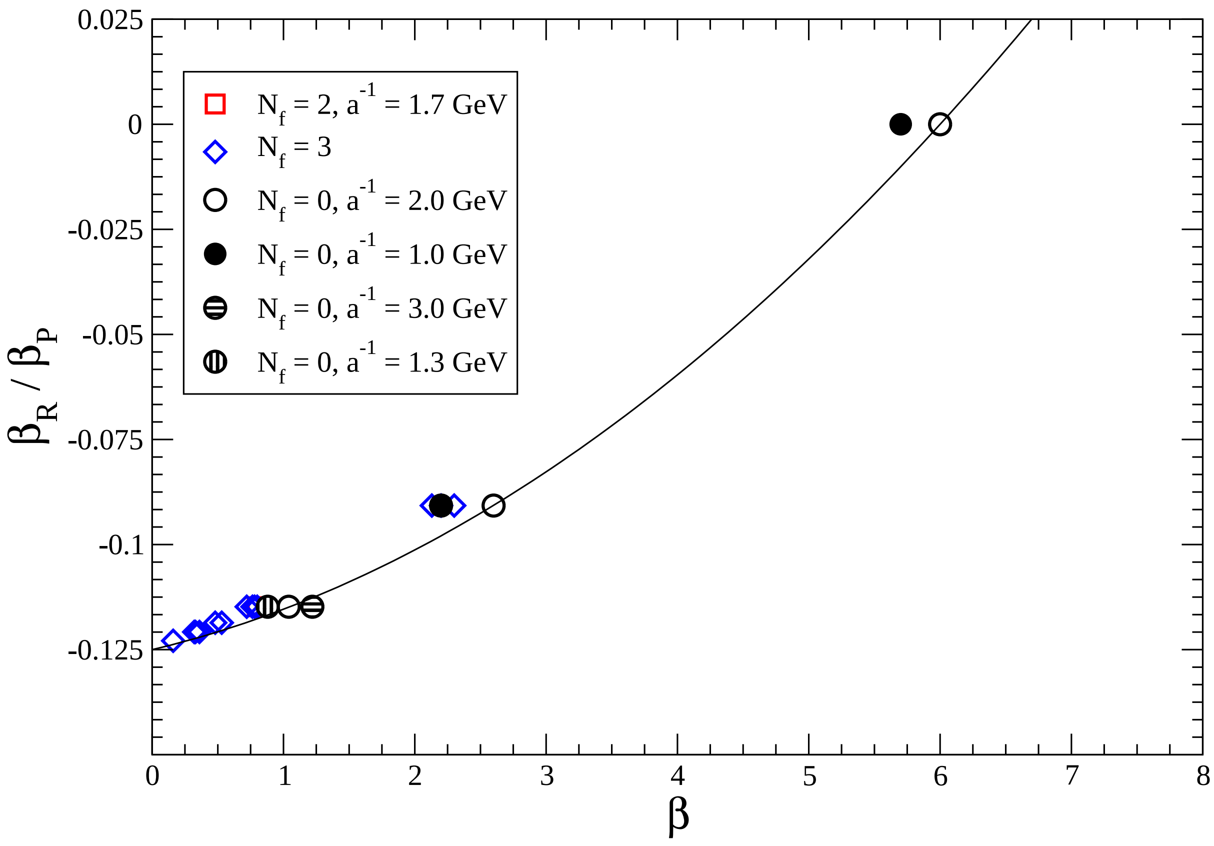

Action Improvement

Exploration of Rectangle Space

An exploration of the rectangle space was conducted on small $16^3 \times 32$ 3-flavor lattices. Runs focused on the high-rectangle region.

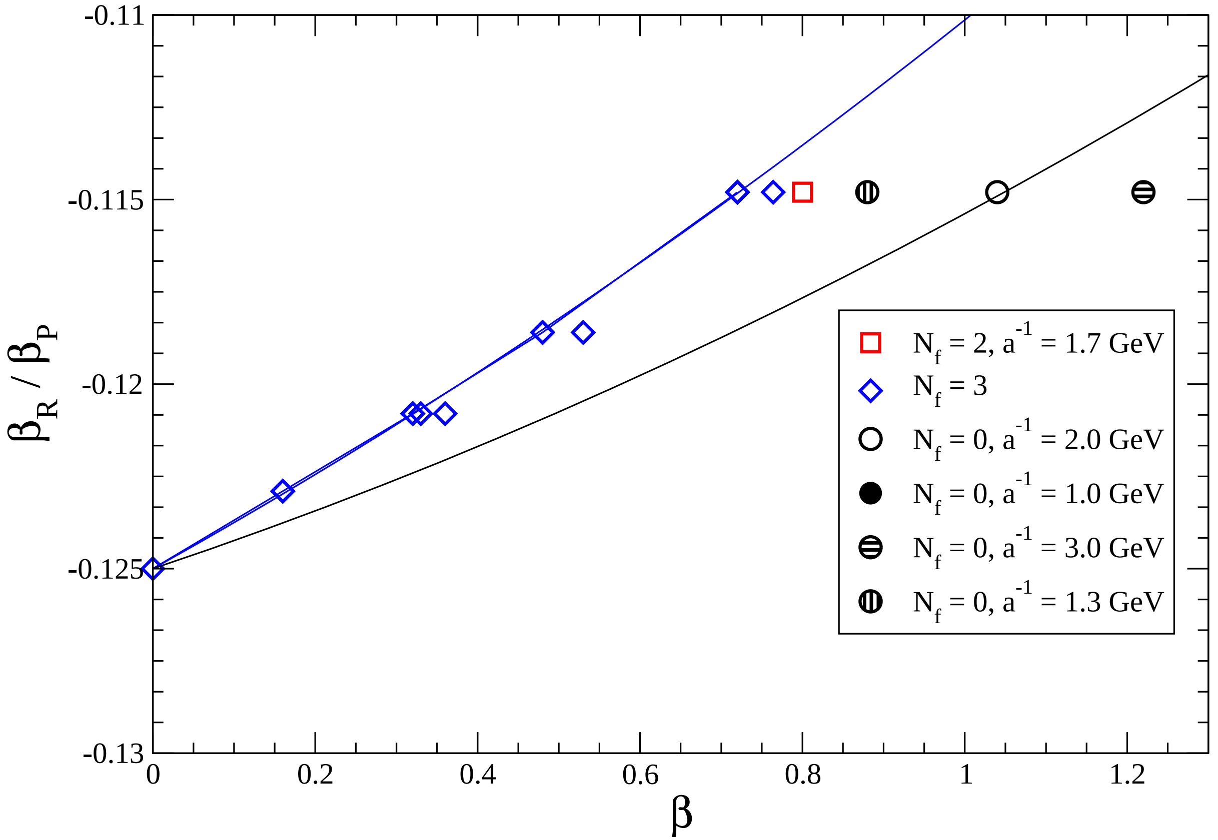

Action Improvement

Exploration of Rectangle Space

As expected, along a line of constant lattice scale, residual mass decreases as the rectangle coefficient increases.

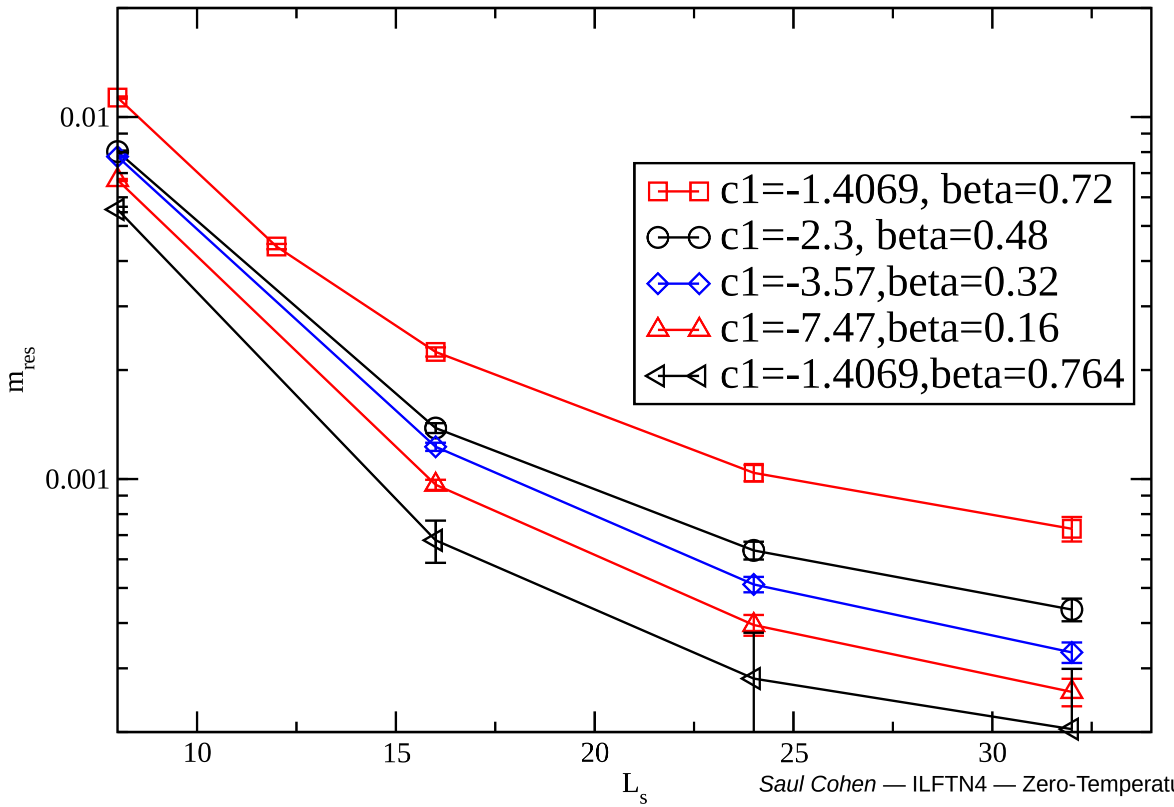

Action Improvement

Topology Change

However, suppressing spatially small gauge fluctuations suppresses the rate at which the topology of the lattice changes. Large rectangle terms essentially freeze the topological charge.

Compromise

To balance these competing effects, we select a small, nonzero rectangle term, $c_1 = -0.331$, the Iwasaki action. Extensive runs at small volume were also made using the larger rectangle term $c_1 = -1.4069$ of the DBW2 action.

Algorithm

Hybrid Monte Carlo

The basis of our algorithm is the Hybrid Monte Carlo (HMC) algorithm. In this algorithm, the gauge field is treated like a canonical position in some high-dimensional parameter space. A set of corresponding canonical momenta are generated, and the gauge fields evolve in simulation time along trajectories determined by the overall Hamiltonian.

$$\begin{aligned} Z &= \int [dU][d\Pi][d\bar{\psi}][d\psi]e^{-H} \\ &= \int [dU][d\Pi][d\bar{\psi}][d\psi]e^{-\Pi^2-S} \end{aligned}$$

Algorithm

Hybrid Monte Carlo

The basis of our algorithm is the Hybrid Monte Carlo (HMC) algorithm. In this algorithm, the gauge field is treated like a canonical position in some high-dimensional parameter space. A set of corresponding canonical momenta are generated, and the gauge fields evolve in simulation time along trajectories determined by the overall Hamiltonian.

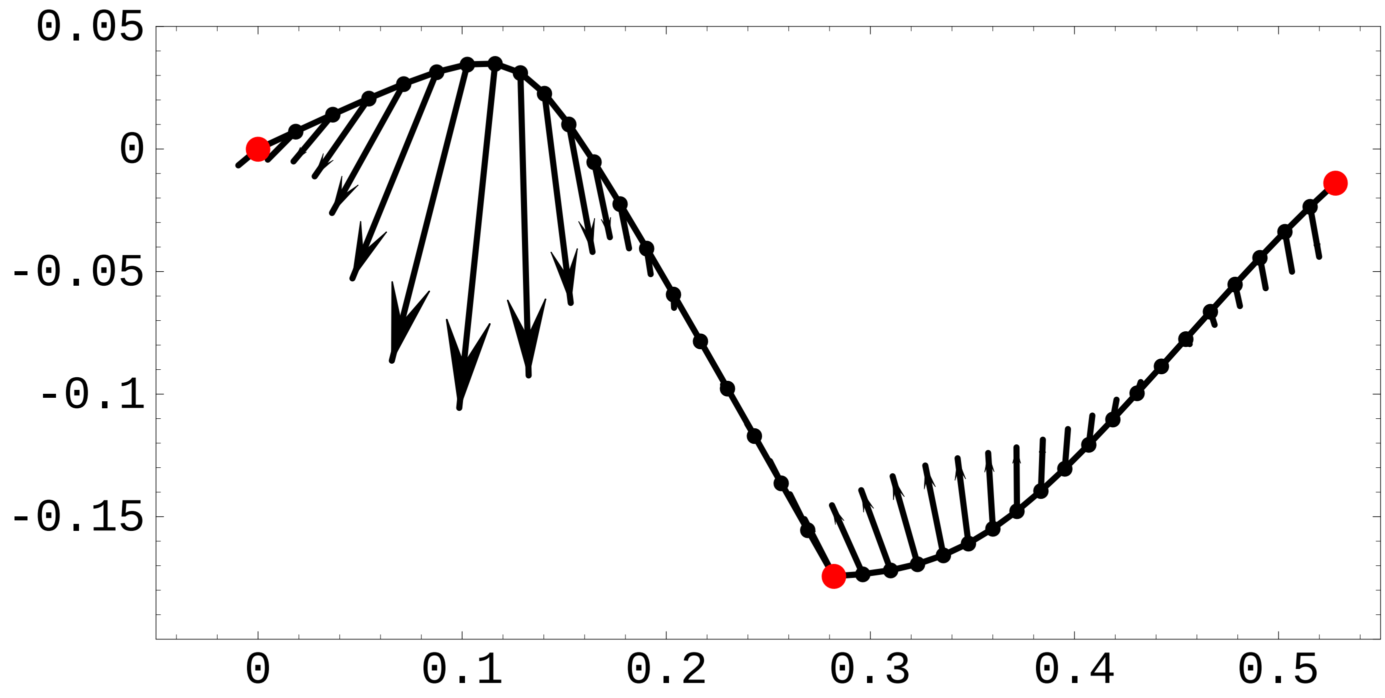

Algorithm

Pseudofermions

Total action combines the gauge action (Iwasaki) with a pseudofermion calculation of the fermionic determinant.

$$\begin{aligned} Z &= \int [dU][d\Pi]\, \det(\not{D} + m) e^{-\Pi^2 - S_g} \\ &= \int [dU][d\Pi][d\phi^*][d\phi] e^{-\Pi^2 - S_g + \phi^* (\not{D}+m)^{-1} \phi} \end{aligned}$$

Pauli-Villars Fields

In the DWF formulation, we do not wish to see unphysical bulk modes. These may be cancelled by the addition of massive pseudofermion fields.

$$Z = \int [dU][d\Pi][d\phi^*][d\phi][d\chi^*][d\chi] e^{-\Pi^2 - S_g + \phi^* (\not{D}+m)^{-1} \phi + \chi^* (\not{D}+1) \chi}$$

Algorithm Improvement

Rational Hybrid Monte Carlo

Rather than directly computing the determinant of an operator, we may use a rational approximation. See Clark, de Forcrand and Kennedy (hep-lat/0510004).

$$\begin{aligned} \det \mathcal{M} &= \int [d\phi^*][d\phi] e^{-\phi^* \mathcal{M}^{-\alpha} \phi} \\ &= \int [d\phi^*][d\phi] e^{-\phi^* r^2(\mathcal{M}) \phi}, \end{aligned}$$

where

$$r(x) = \sum_{k=1}^{n} \frac{\alpha_k}{x + \beta_k} \approx x^{-\alpha/2}.$$

– The convergence of the conjugate gradient for each pole of the rational approximation may be separately tuned. All poles are solved simultaneously thanks to the multishift solver.

Algorithm Improvement

Quotient Hybrid Monte Carlo

When simulating multiple fermion fields and Pauli-Villars pseudofermions, the Pauli-Villars fields will cancel unphysical modes only stochastically. Combining two determinants into a single term reduces this noise contribution.

$$
\begin{aligned}
\sqrt{\frac{\det \mathcal{M}_f^\dagger \mathcal{M}_f}{\det \mathcal{M}_{\mathrm{PV}}^\dagger \mathcal{M}_{\mathrm{PV}}}} &= \det\left[(\mathcal{M}_{\mathrm{PV}}^\dagger \mathcal{M}_{\mathrm{PV}})^{-1/8}(\mathcal{M}_f^\dagger \mathcal{M}_f)^{1/4}(\mathcal{M}_{\mathrm{PV}}^\dagger \mathcal{M}_{\mathrm{PV}})^{-1/8}\right]^2 \\
&= \int [d\phi^*][d\phi] e^{-\phi^*\left[(\mathcal{M}_{\mathrm{PV}}^\dagger \mathcal{M}_{\mathrm{PV}})^{-1/8}(\mathcal{M}_f^\dagger \mathcal{M}_f)^{1/4}(\mathcal{M}_{\mathrm{PV}}^\dagger \mathcal{M}_{\mathrm{PV}})^{-1/8}\right]^2 \phi}
\end{aligned}
$$

Algorithm Improvement

Quotient Rational Hybrid Monte Carlo

This may then be combined with the RHMC technique, using a separate rational approximation for each operator.

$$\sqrt{\frac{\det \mathcal{M}_f^\dagger \mathcal{M}_f}{\det \mathcal{M}_{\mathrm{PV}}^\dagger \mathcal{M}_{\mathrm{PV}}}} = \int [d\phi^*][d\phi] e^{-\phi^* \left[(\mathcal{M}_{\mathrm{PV}}^\dagger \mathcal{M}_{\mathrm{PV}})^{-1/8} (\mathcal{M}_f^\dagger \mathcal{M}_f)^{1/4} (\mathcal{M}_{\mathrm{PV}}^\dagger \mathcal{M}_{\mathrm{PV}})^{-1/8} \right]^2 \phi}$$

$$= \int [d\phi^*][d\phi] e^{-\phi^* \left[r_1(\mathcal{M}_{\mathrm{PV}}^\dagger \mathcal{M}_{\mathrm{PV}}) r_2(\mathcal{M}_f^\dagger \mathcal{M}_f) r_1(\mathcal{M}_{\mathrm{PV}}^\dagger \mathcal{M}_{\mathrm{PV}}) \right]^2 \phi}$$

– The choice of which fermions masses appear in each numerator and denominator may be tuned.

Algorithm Improvement

Leapfrog Integrator

A naive scheme of updating $T(\Pi)$ and $V(U)$ together at each timestep in a trajectory may easily be improved by updating the canonical position and momentum at alternate half-timesteps.

$$e^{\delta\tau(T+V)} \longrightarrow e^{\frac{\delta\tau}{2}T} e^{\delta\tau V} e^{\frac{\delta\tau}{2}T} + \mathcal{O}\left(\delta\tau^3\right)$$

Multiple Timescale Integrator

The various contributions to T and V need not be calculated equally frequently. Cheap or important contributions, such as the gauge force term, may be updated more often.

Algorithm Improvement

Omelyan Integrator

This scheme may be further improved by splitting up the updates further. Such a scheme increases the number of times the force must be evaluated, but may increase acceptance so much that it increases overall speed. Such a scheme was studied by Takaishi and de Forcrand (hep-lat/0505020).

$$e^{\delta\tau(T+V)} \longrightarrow e^{\lambda\delta\tau V} e^{\frac{\delta\tau}{2}T} e^{(1-2\lambda)\delta\tau V} e^{\frac{\delta\tau}{2}T} e^{\lambda\delta\tau V} + \mathcal{O}\left(\delta\tau^3\right)$$

– The parameter $\lambda \approx 0.193$ may be tuned to reduce error in the Hamiltonian.

Parameter Tuning

Initial Omelyan Parameter

From Omelyan's theoretical arguments, we expect λ should be 0.193. Further refined by study on $16^3 \times 32$ lattices.

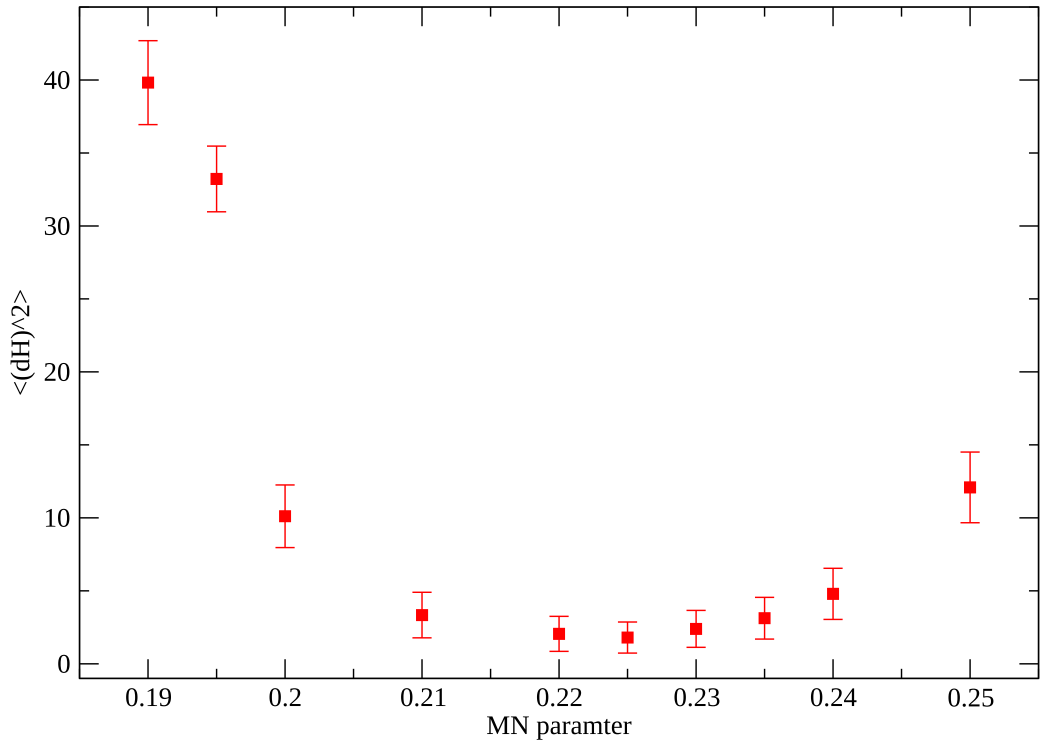

Parameter Tuning

Baseline

dim	$24^3 \times 64$	β	2.13
L_s	16	c_1	-0.331 (Iwasaki)

m_s	0.04	m_l	0.02	m_{PV}	1.0

Multiscale RHMC without quotient force term

HMC masses	RHMC masses	RHMC powers	λ	$\delta\tau$	δH	Total CG
1.0 (2 bosons)	0.02 0.02 0.04 1.0	$\frac{1}{2}$ $\frac{1}{2}$ $\frac{1}{2}$ $-\frac{1}{2}$	0.225	1/15	0.579	194,303

Parameter Tuning

QRHMC

Just the Quotient force term yields a factor of almost 4 in CG count.

HMC masses	RHMC masses	RHMC powers	λ	$\delta\tau$	δH	Total CG
0.02/1.0	0.04/1.0	1/2	0.225	1/15	504.0	42,103
0.02/1.0	0.04/1.0	1/2	0.225	1/20	4.571	56,327
0.02/1.0	0.04/1.0	1/2	0.220	1/20	6.765	56,267
0.02/1.0	0.04/1.0	1/2	0.230	1/20	5.782	56,293

Quotient HMC+RHMC without Hasenbush-style preconditioning

Parameter Tuning

QRHMC with Preconditioning

Preconditioning allows further relaxation of $\delta\tau$.

HMC masses	RHMC masses	RHMC powers	λ	$\delta\tau$	δH	Total CG
0.02/0.04	0.04/1.0, 0.04/1.0	3/4, 3/4	0.225	1/20	-0.0419	77,122
0.02/0.04	0.04/1.0, 0.04/1.0	3/4, 3/4	0.225	1/10	1.193	41,041
0.02/0.04	0.04/1.0, 0.04/1.0	3/4, 3/4	0.225	1/12	0.351	46,457
0.02/0.04	0.04/0.1, 0.04/0.1	3/4, 3/4				
	0.1/1.0, 0.1/1.0	3/4, 3/4	0.225	1/12	-2.168	76,348
0.02/0.04	0.04/1.0, 0.04/1.0	3/4, 3/4	0.220	1/10	0.835	41,155
0.02/0.04	0.04/1.0, 0.04/1.0	3/4, 3/4	0.215	1/10	0.500	41,242

Quotient HMC+RHMC with Hasenbush-style preconditioning

Parameter Tuning

Multiple Timescales and Stopping Conditions

Adjusting the timescales and stopping conditions of the HMC and RHMC separately yields another factor of about 2.

0.02/0.04 masses	0.04/1.0 masses	A_steps	λ	$\delta\tau$	δH force	Total CG
		H_R_G evolution				
HMC	2 $\times$ RHMC(3/4)	1	0.215	1/5	0.798	34,819
			HMC	0.1	6.0	
			RHMC	0.0215	35	
			RHMC	0.043	70	
			RHMC	0.057	92	

Parameter Tuning

Multiple Timescales and Stopping Conditions

Adjusting the timescales and stopping conditions of the HMC and RHMC separately yields another factor of about 2.

0.02/0.04 masses	0.04/1.0 masses	A_steps	λ	$\delta\tau$	δH force	Total CG
H_R_G: 10^{-7} MD CG stop RHMC, 10^{-6} MD CG stop HMC						
HMC	$3 \times$ RHMC(1/2)	1	0.215	1/3	0.0130	33,777
			HMC	0.16667	9.8	
			RHMC	0.035833	37	
			RHMC	0.071667	75	
			RHMC	0.095	99	

Parameter Tuning

Multiple Timescales and Stopping Conditions

Adjusting the timescales and stopping conditions of the HMC and RHMC separately yields another factor of about 2.

0.02/0.04 masses	0.04/1.0 masses	A_steps	λ	$\delta\tau$	δH force	Total CG
	H_R_G: 10^{-5} MD CG stop RHMC, 10^{-6} MD CG stop HMC					
HMC	$3 \times$ RHMC(1/2)	1	0.215	1/3	0.0698	24,659
			HMC	0.16667	9.8	
			RHMC	0.035833	37	
			RHMC	0.071667	75	
			RHMC	0.095	99	

Parameter Tuning

Multiple Timescales and Stopping Conditions

Adjusting the timescales and stopping conditions of the HMC and RHMC separately yields another factor of about 2.

0.02/0.04 masses	0.04/1.0 masses	A_steps	λ	$\delta\tau$	δH force	Total CG
H_R_G: 10^{-4} MD CG stop RHMC, 10^{-6} MD CG stop HMC						
HMC	$3 \times$ RHMC(1/2)	1	0.215	1/3	0.616	20,107
			HMC	0.16667	9.8	
			RHMC	0.035833	37	
			RHMC	0.071667	75	
			RHMC	0.095	99	

Parameter Tuning

Individual Pole Stopping Conditions

Since the multishift solver works on all poles at once, acceptance may be improved at no cost by tightening bounds on the easy poles.

Fermion Pole	MD stop	0.02/0.04 run CG iters	0.03/0.04 run CG iters
0	2×10^{-5}	207	208
1	2×10^{-6}	211	212
2	2×10^{-7}	180	179
3	1×10^{-7}	114	114
4	1×10^{-7}	66	66
5	1×10^{-7}	38	38
6	1×10^{-7}	22	22
7	1×10^{-7}	12	12
8	1×10^{-7}	6	6

Parameter Tuning

Individual Pole Stopping Conditions

Since the multishift solver works on all poles at once, acceptance may be improved at no cost by tightening bounds on the easy poles.

Boson Pole	MD stop	0.02/0.04 run CG iters	0.03/0.04 run CG iters
0	2×10^{-5}	53	53
1	2×10^{-6}	47	48
2	2×10^{-7}	34	34
3	1×10^{-7}	20	20
4	1×10^{-7}	10	10
5	1×10^{-7}	4	4

Parameter Tuning

Individual Pole Stopping Conditions

Since the multishift solver works on all poles at once, acceptance may be improved at no cost by tightening bounds on the easy poles.

	0.02/0.04 run	0.03/0.04 run
Trajectories	65	35
δH	0.36(12)	0.31(19)
e^{-H}	0.93(12)	0.92(10)
Acceptance	0.74(8)	0.77(12)
CG iter per traj	31,600	30,300
Time per 5 traj	3:07	3:03

Stopping conditions and run information for the $24^3 \times 64 \times 16$, Iwasaki = 2.13, DWF jobs running at BNL. The quotient HMC and RHMC are used in with an H-R-G integration scheme.

Lattice Properties

Run Progress

Production $24^3 \times 64 \times 16$ lattices are well underway. Basic parameters, production speed, plaquette and $\overline{\psi}\psi$ evolution.

Spectrum and Residual Mass

Meson spectrum and residual mass have been measured on the lattices already.

Decay Constant and Scale Setting

Decay constant may be used to set the scale until better vector plateaux and heavy-quark potential are available.

Run Progress

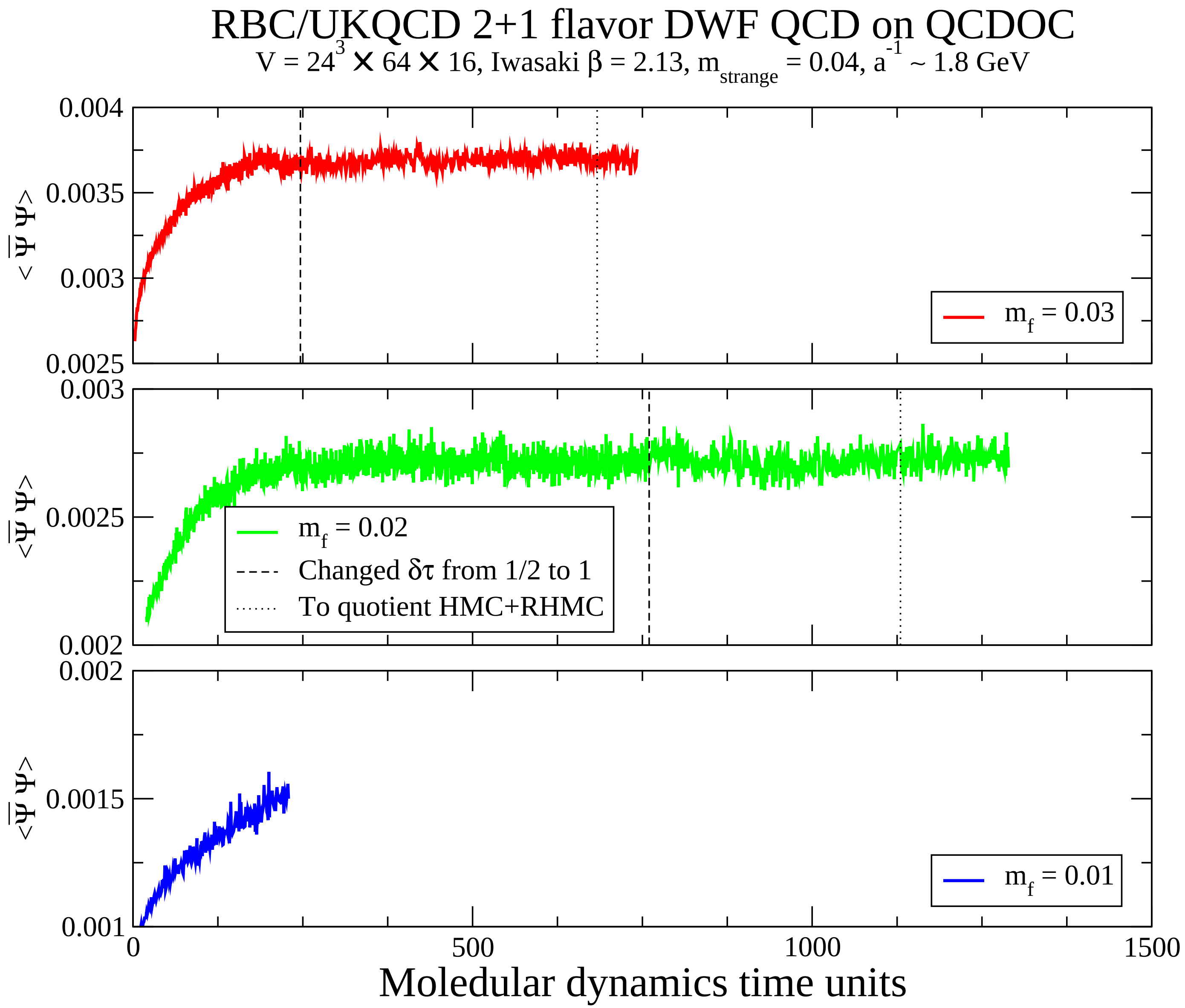

Run Progress

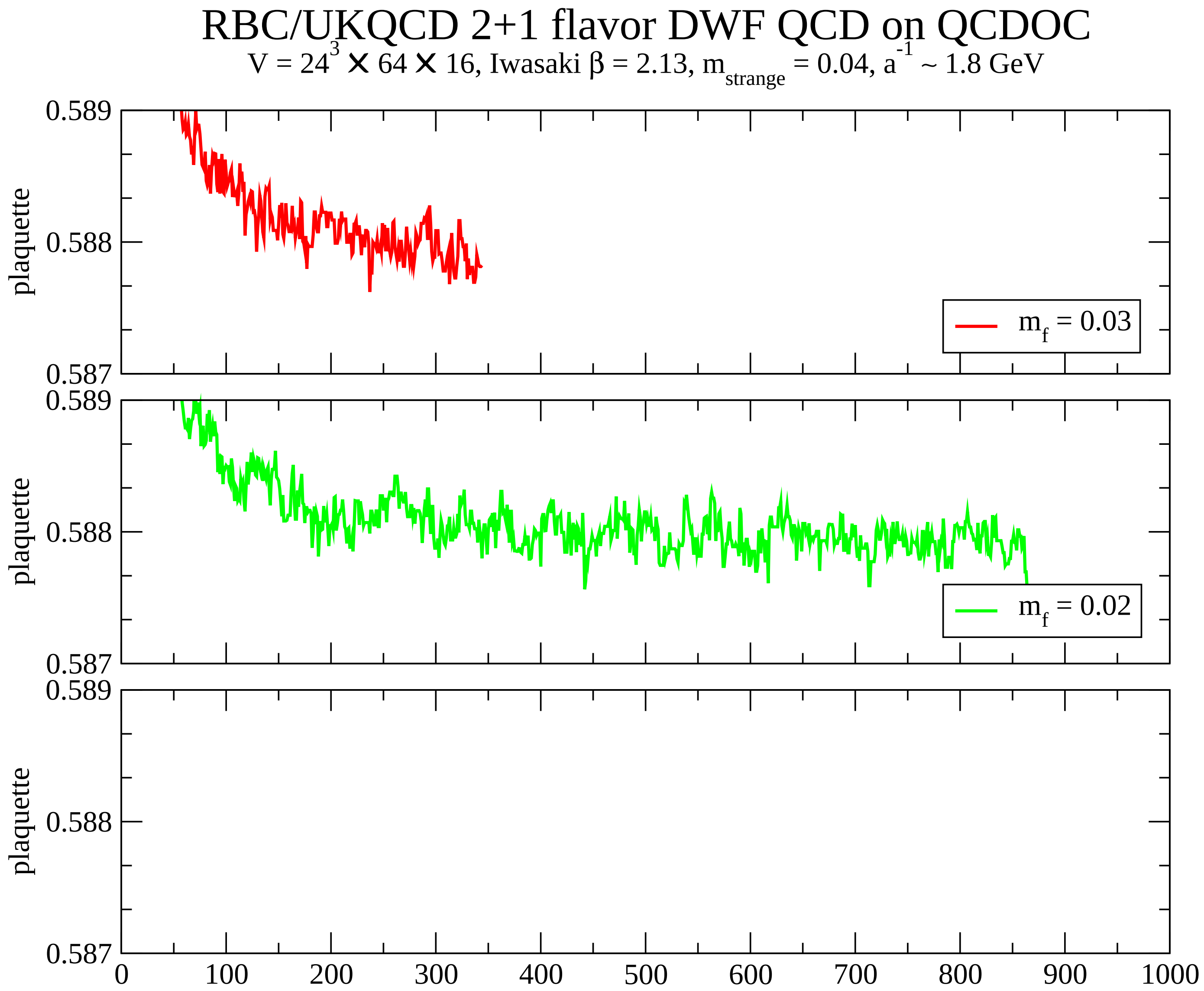

Caveat: Older partial measurements.

Measurements

Residual Mass

Residual mass is around 1/3 of our lightest quark mass.

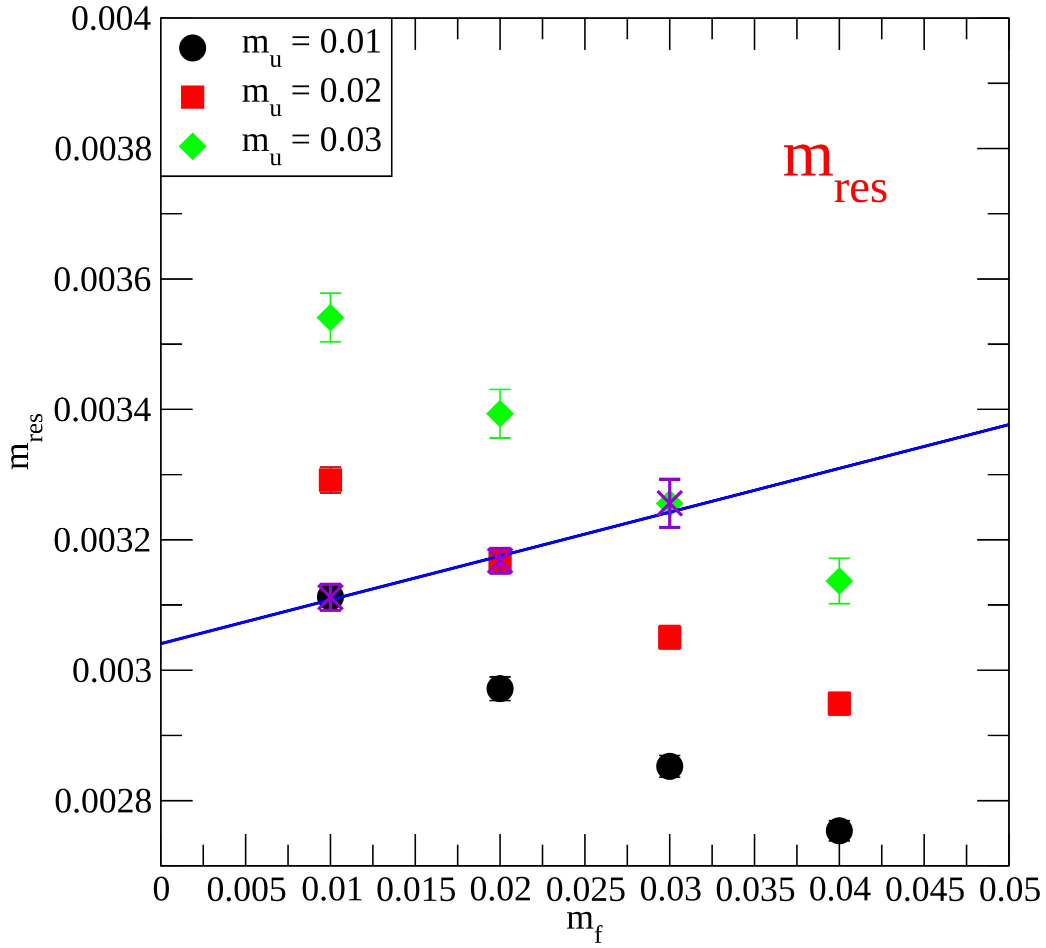

Measurements

Pseudoscalar Mass

The pseudoscalar is very clean.

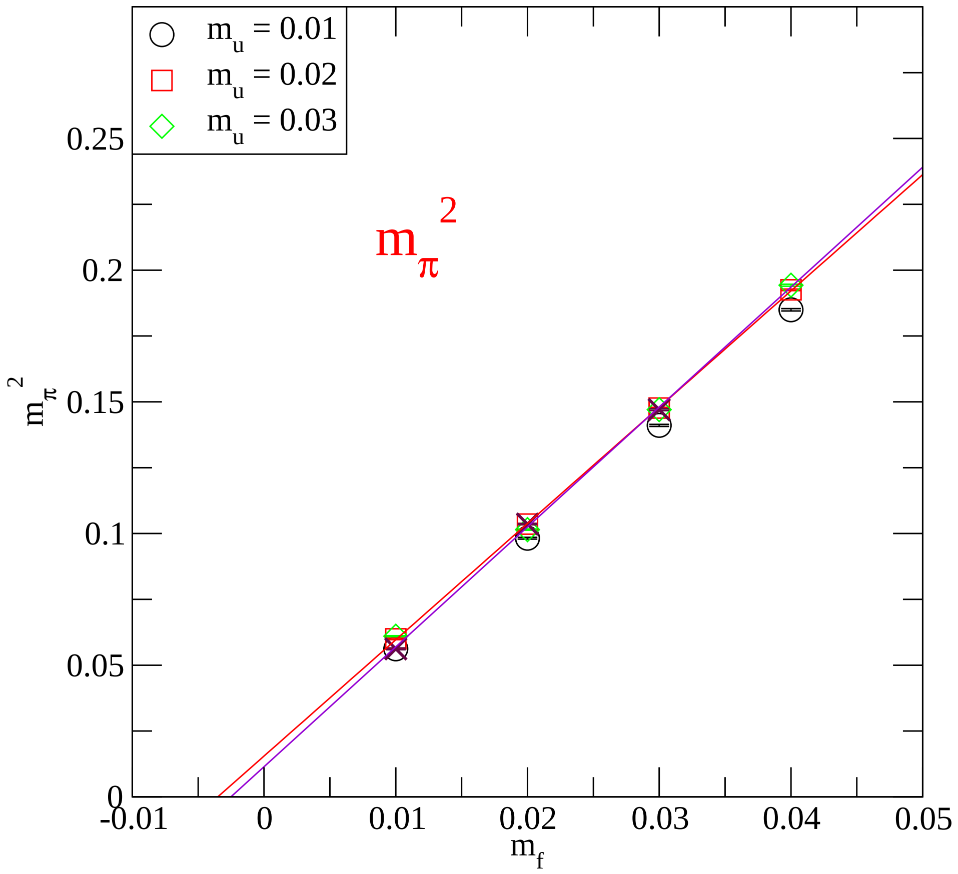

Measurements

Pseudoscalar Mass

The pseudoscalar is very clean. Plateaux are somewhat improved by selection of box size. 16^3 seems to be about the right size.

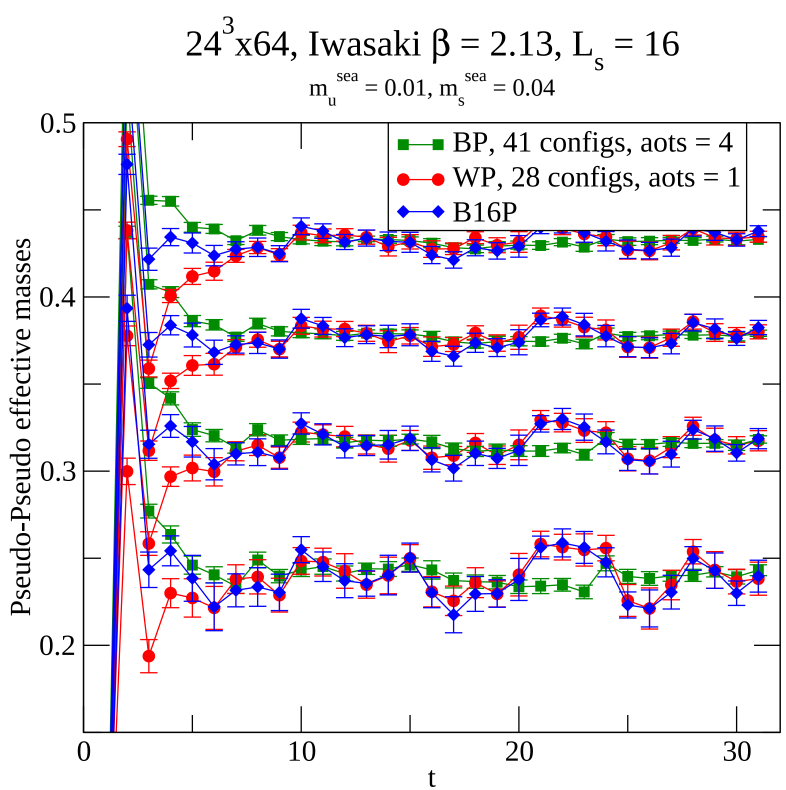

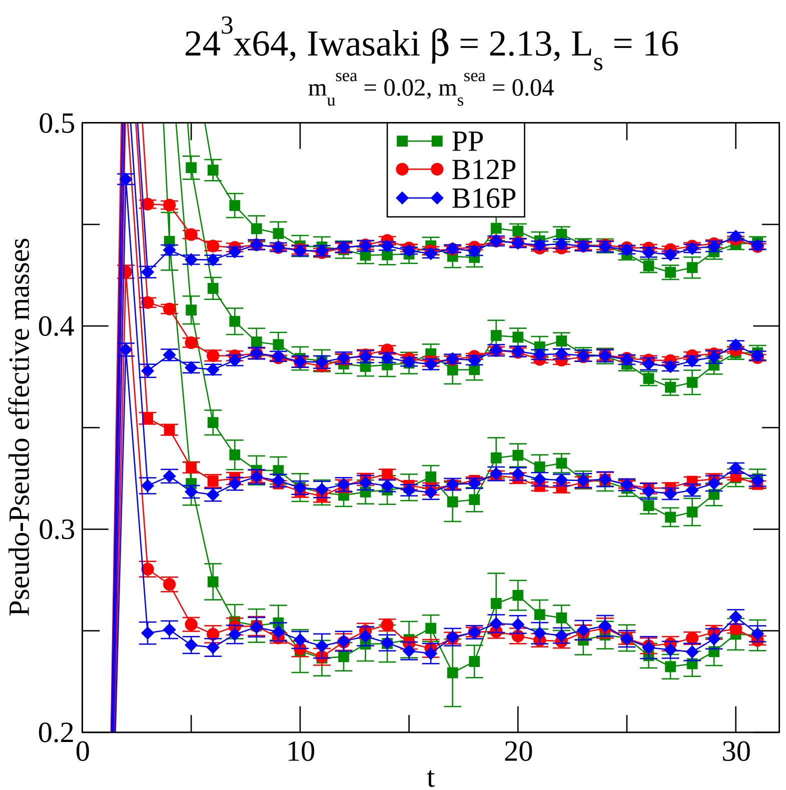

Measurements

Vector Mass

The vector is a bit more challenging.

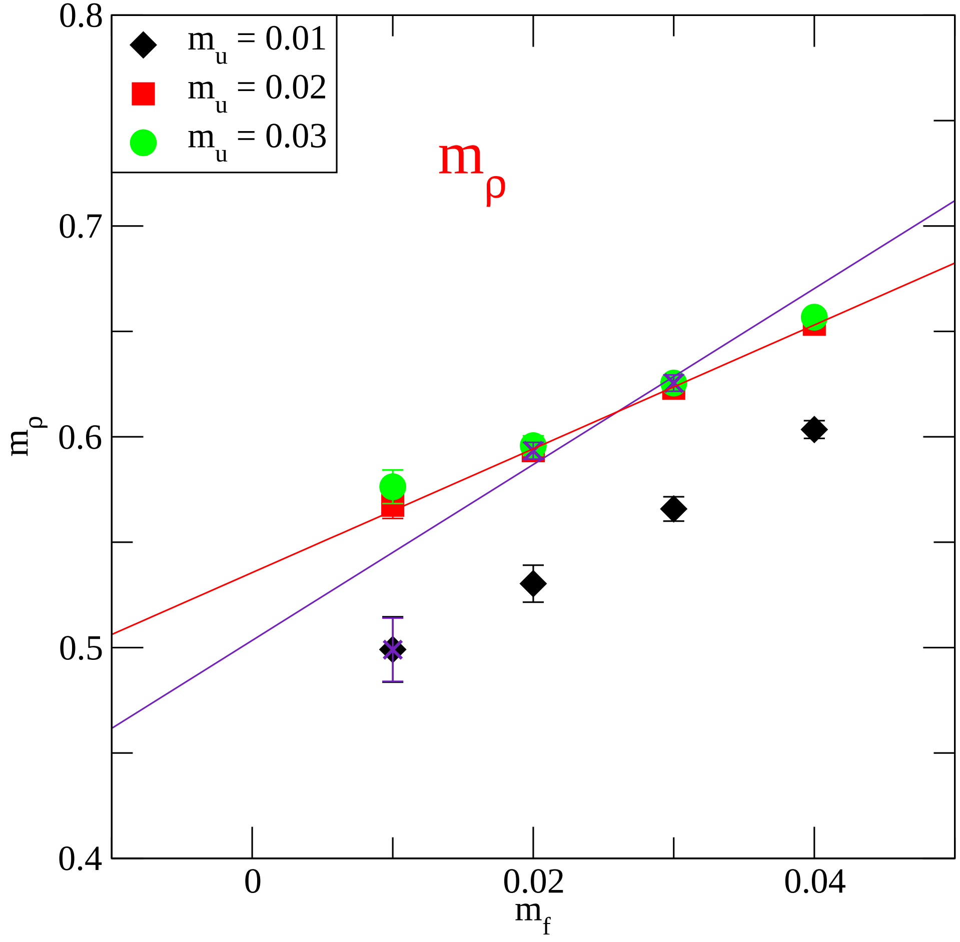

Measurements

Vector Mass

The vector is a bit more challenging. Tuning the box size seems to help a bit.

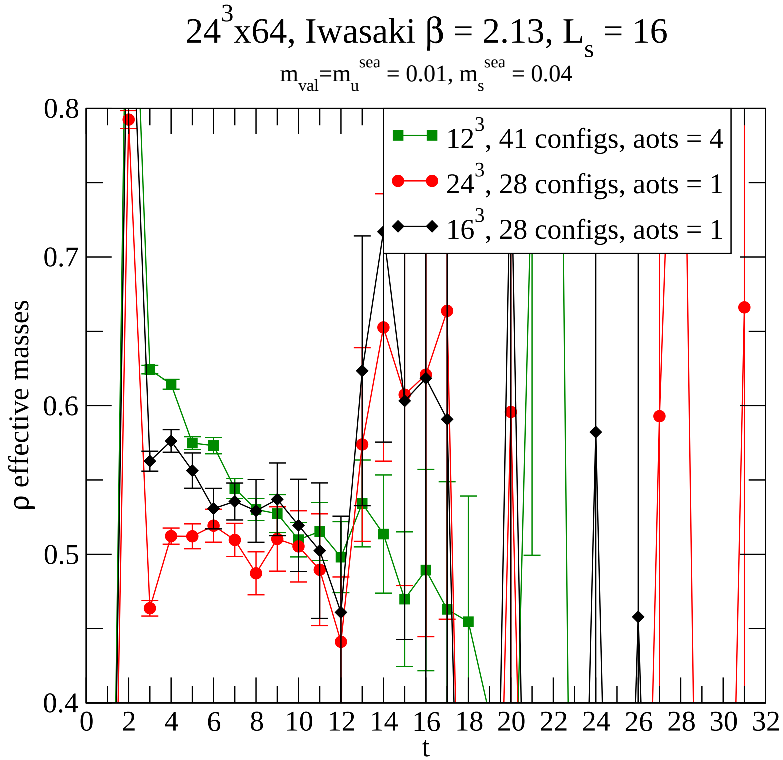

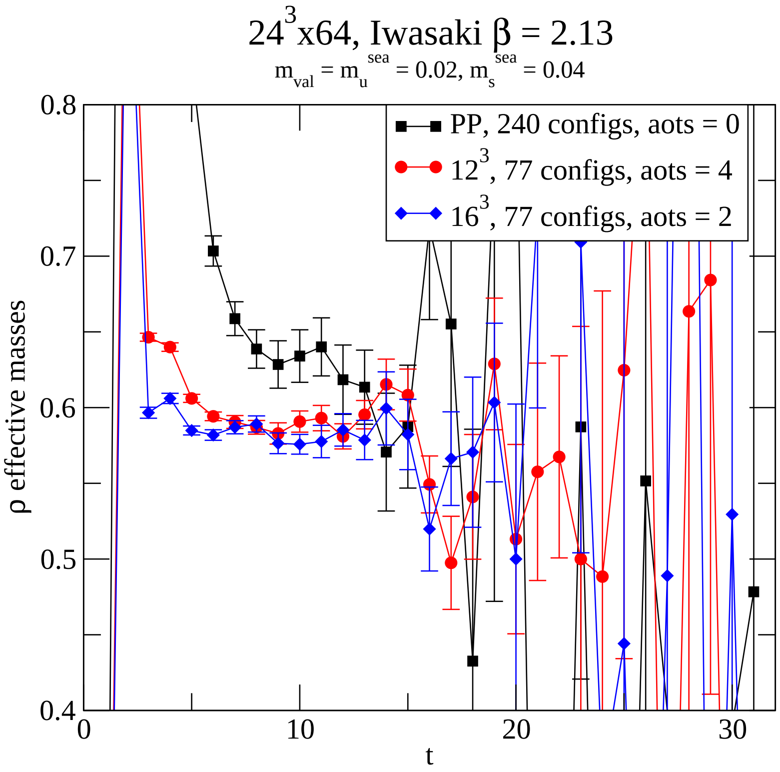

Measurements

Z_A

Z_A is needed to correctly apply the Ward identity to our correlators.

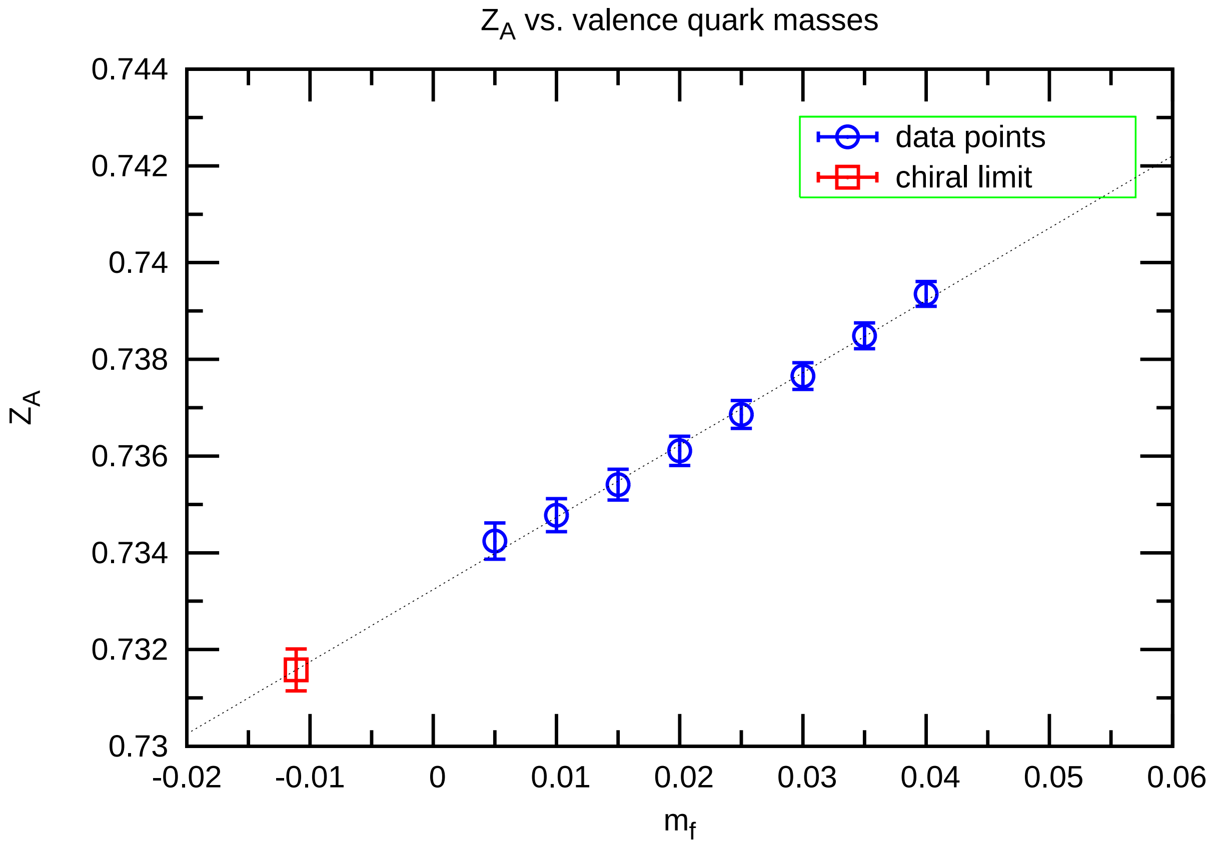

Measurements

f_π

The pseudoscalar decay constant may be determined from a combination of wall-point or point-point correlators.

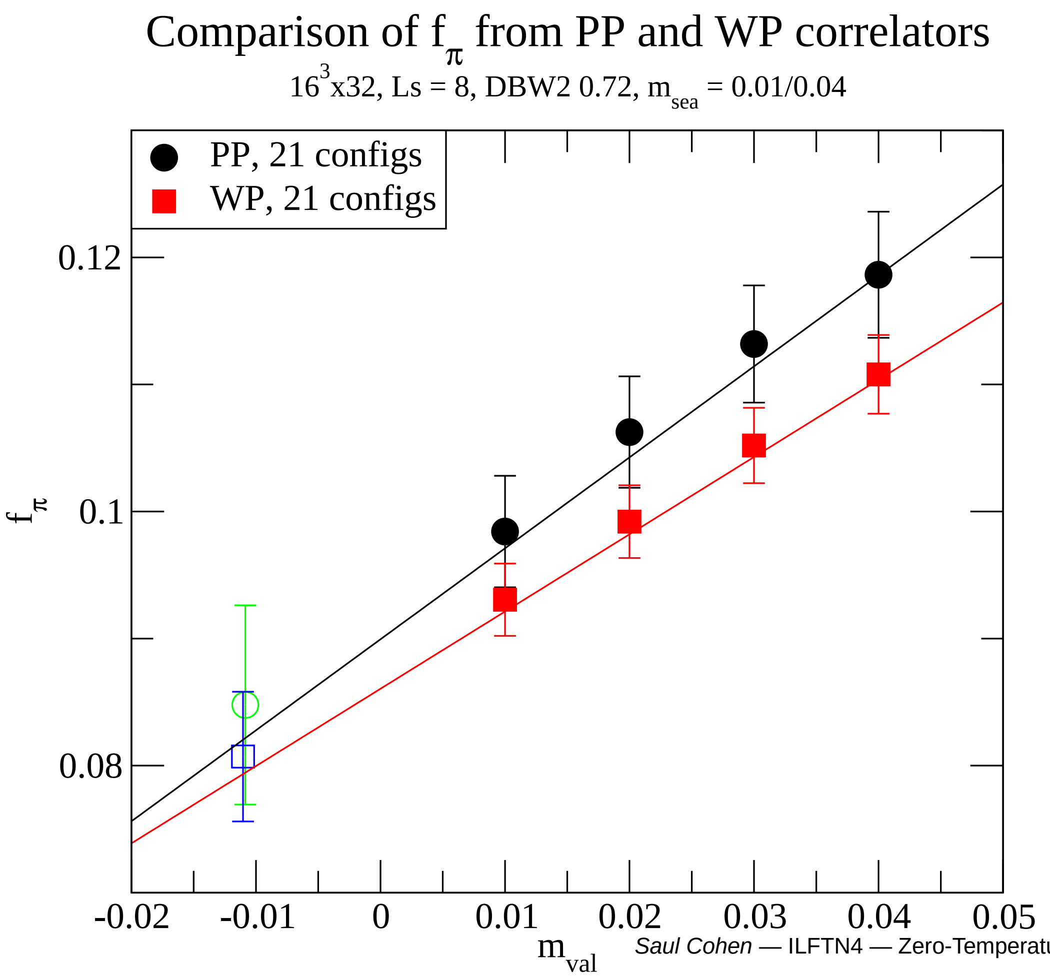

Lattice Calculations

Kaon Bag Parameter

Preliminary results from $16^3 \times 32$ lattices.

Chiral fi tting

Sharpe & van de Water's chiral form for 2+1 flavors in continuum may be applied.

Convolved source

On larger lattices, wall source is too large to overlap with realistic meson states. Box sources induce higher-momentum states. Convolved box source projects to zero momentum.

Kaon Bag Parameter

Important to CP Violation

Errors in the determination of ϵ are now dominated by uncertainty in the value of B_K.

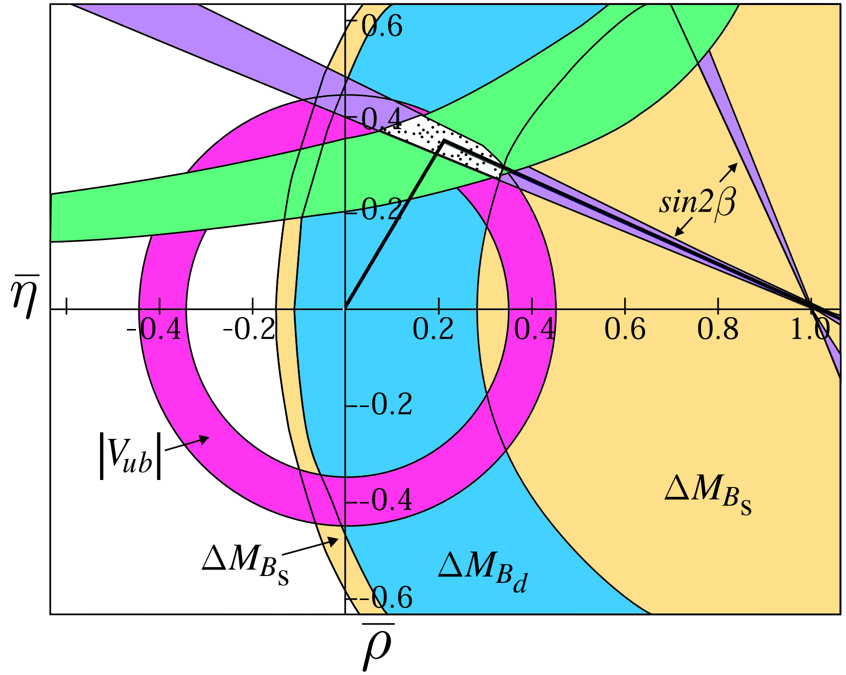

$$\epsilon = \hat{\mathbf{B}}_{\mathbf{K}}\, \mathrm{Im}\lambda_t \frac{G_F^2 f_K^2 M_K M_W^2}{6\sqrt{2}\pi^2 \Delta M_K}$$
$$\times \{\mathrm{Re}\lambda_c [\eta_1 S_0(x_c) - \eta_3 S_0(x_c, x_t)] - \mathrm{Re}\lambda_t\, \eta_2 S_0(x_t)\}\, e^{i\pi/4}$$

Constraint by ϵ denoted by green hyperbolic bands.

Kaon Bag Parameter

Definition

B_K parametrizes the amount of mixing between neutral kaons due to weak interactions:

$$B_K = \frac{\langle \bar{K}^0 | \mathcal{O}_{LL}^{\Delta S=2} | K^0 \rangle}{\frac{8}{3} f_K^2 M_K^2}$$

$$\mathcal{O}_{LL}^{\Delta S=2} = (\bar{s}d)_L (\bar{s}d)_L$$

Kaon Bag Parameter

Fundamental Interaction

At the fundamental level, we understand this mixing is due to the exchange of two W bosons between the quarks of the kaon.

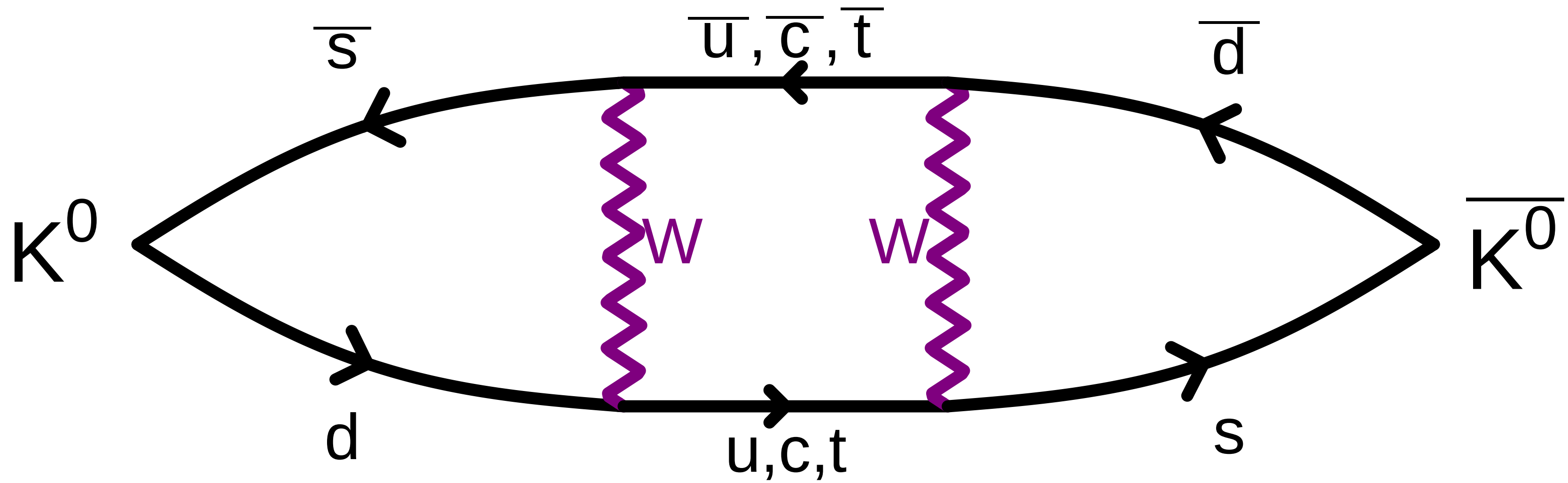

Three-Point Matrix Elements

Figure Eight Diagram

This is the diagram we evaluate for B_K. The operator is inserted at the center of the diagram;

Figure Eight

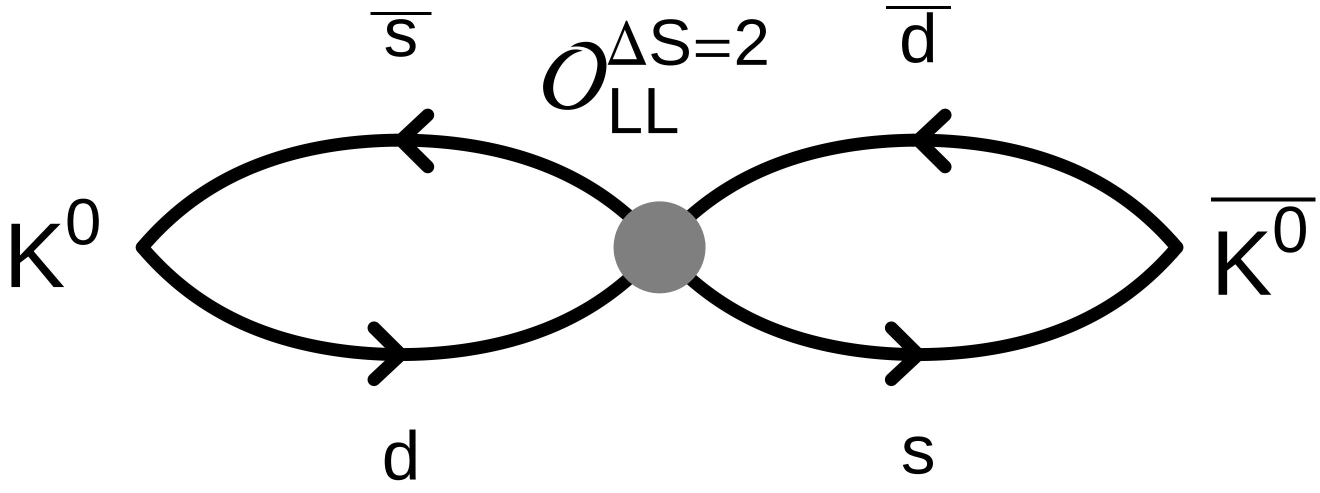

Three-Point Matrix Elements

Figure Eight Diagram

This is the diagram we evaluate for B_K. The operator is inserted at the center of the diagram; spin and color traces may be taken around either the entire figure-eight or around each lobe individually.

One Trace

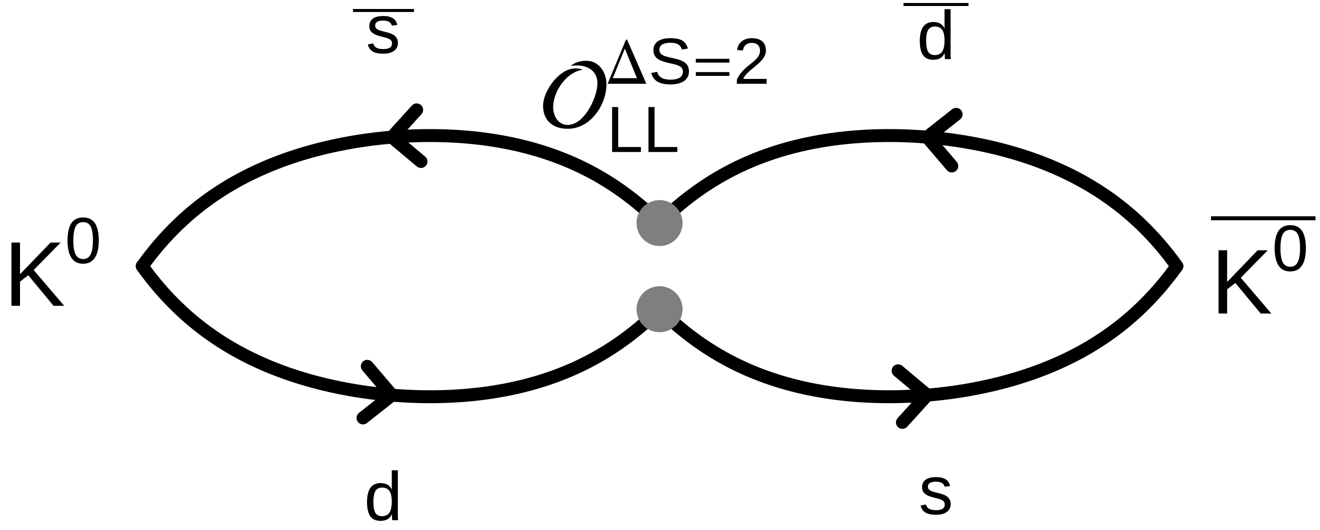

Three-Point Matrix Elements

Figure Eight Diagram

This is the diagram we evaluate for B_K. The operator is inserted at the center of the diagram; spin and color traces may be taken around either the entire figure-eight or around each lobe individually.

Two Traces

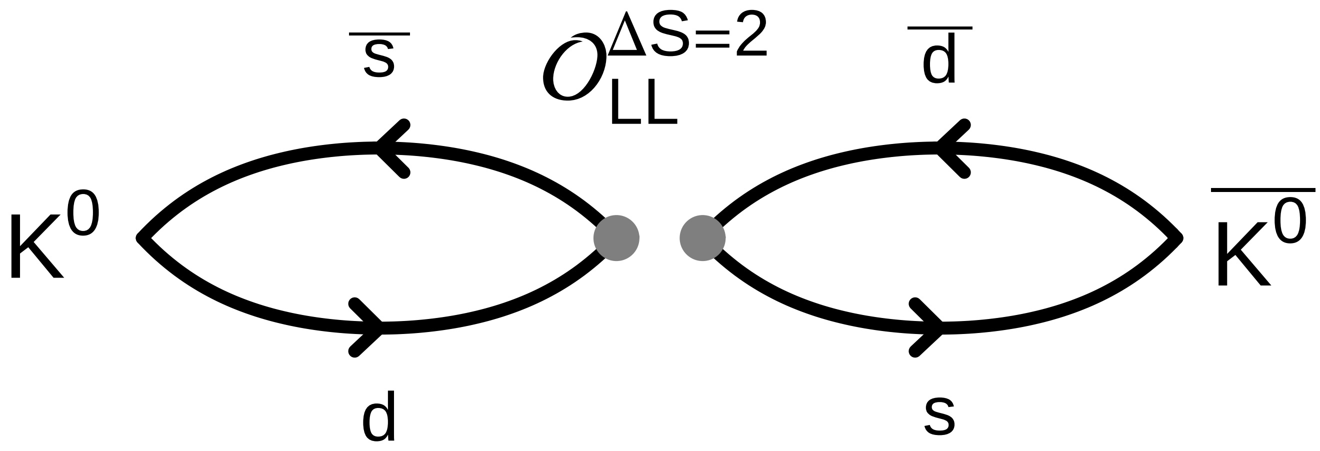

The Bag Parameter

Matrix Element versus Average Quark Mass

The matrix element should go to zero at $-m_{res}$ with a known chiral form $\langle \bar{K^0}|\mathcal{O}^{\Delta S=2}|K^0\rangle = am\left(1 - b\left(\frac{M_P}{4\pi f_P}\right)^2 \log \frac{M_P^2}{\Lambda^2_{\chi\mathrm{PT}}}\right) + cm^2$. The goodness of this fit indicates that chiral symmetry breaking is under control.

$$\left\langle\overline{\mathrm{PS}}\middle|\mathcal{O}_{LL}^{\Delta S=2}\middle|\mathrm{PS}\right\rangle = 4M_P\frac{\mathcal{C}_{wpw}^{P\mathcal{O}P}(t_{\mathrm{src}}, t, t_{\mathrm{snk}})}{\mathcal{C}_{ww}^{PP}(t_{\mathrm{src}}, t_{\mathrm{snk}})}$$

The Bag Parameter

Matrix Element versus Average Quark Mass

The matrix element should go to zero at $-m_{res}$ with a known chiral form $\langle \bar{K^0}|\mathcal{O}^{\Delta S=2}|K^0\rangle = am\left(1 - b\left(\frac{M_P}{4\pi f_P}\right)^2 \log\frac{M_P^2}{\Lambda_{\chi\mathrm{PT}}^2}\right) + cm^2$. The goodness of this fit indicates that chiral symmetry breaking is under control.

Matrix Element

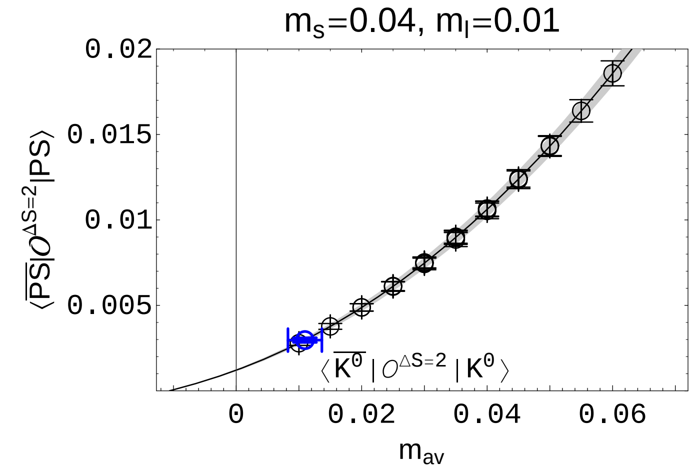

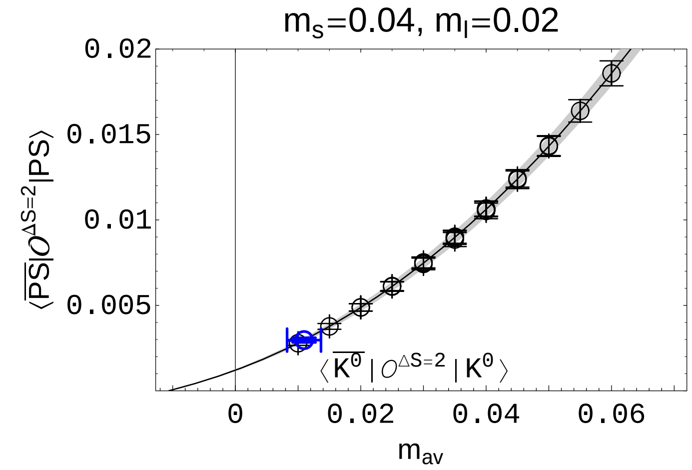

The Bag Parameter

Two Approaches – Naive Approach

$$B_P = \frac{\langle \overline{\mathrm{PS}} | \mathcal{O}_{LL}^{\Delta S=2} | \mathrm{PS} \rangle}{\frac{8}{3} f_K^2 M_K^2}$$

The Bag Parameter

Two Approaches – Naive Approach

$$B_P = \frac{\langle \overline{\mathrm{PS}} | \mathcal{O}_{LL}^{\Delta S=2} | \mathrm{PS} \rangle}{\frac{8}{3} f_K^2 M_K^2}$$

Bag Parameter

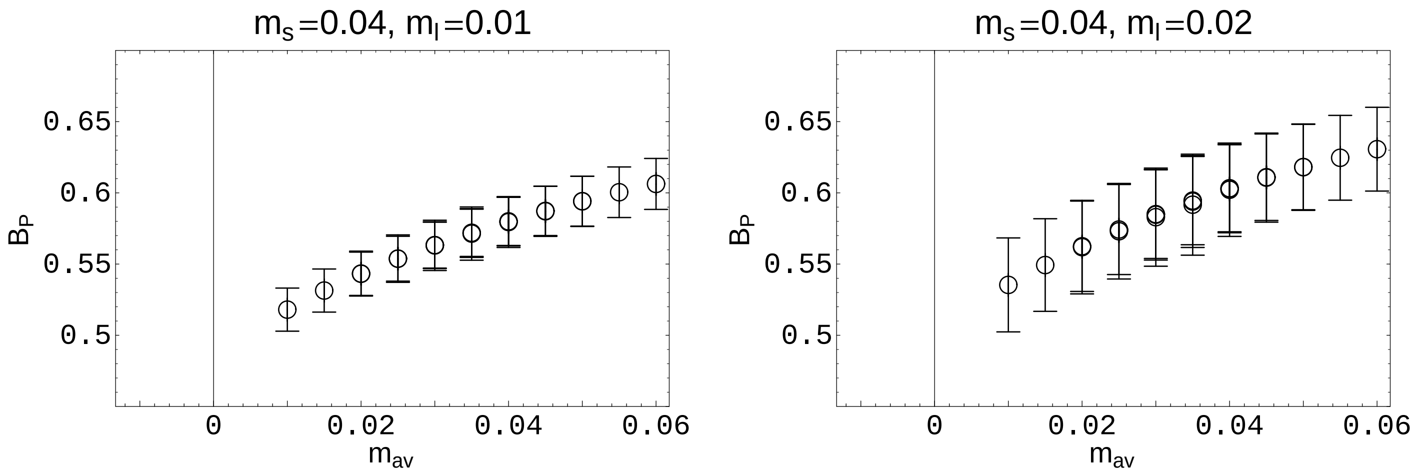

The Bag Parameter

Two Approaches – Clever Approach

$$B_P = \frac{M_P^2 V}{2\frac{8}{3}(m_q + m_{\rm res})^2} \frac{\mathcal{C}_{wpw}^{POP}(t_{\rm src}, t, t_{\rm snk})}{\mathcal{C}_{wp}^{PP}(t_{\rm src}, t)\mathcal{C}_{wp}^{PP}(t, t_{\rm snk})}$$

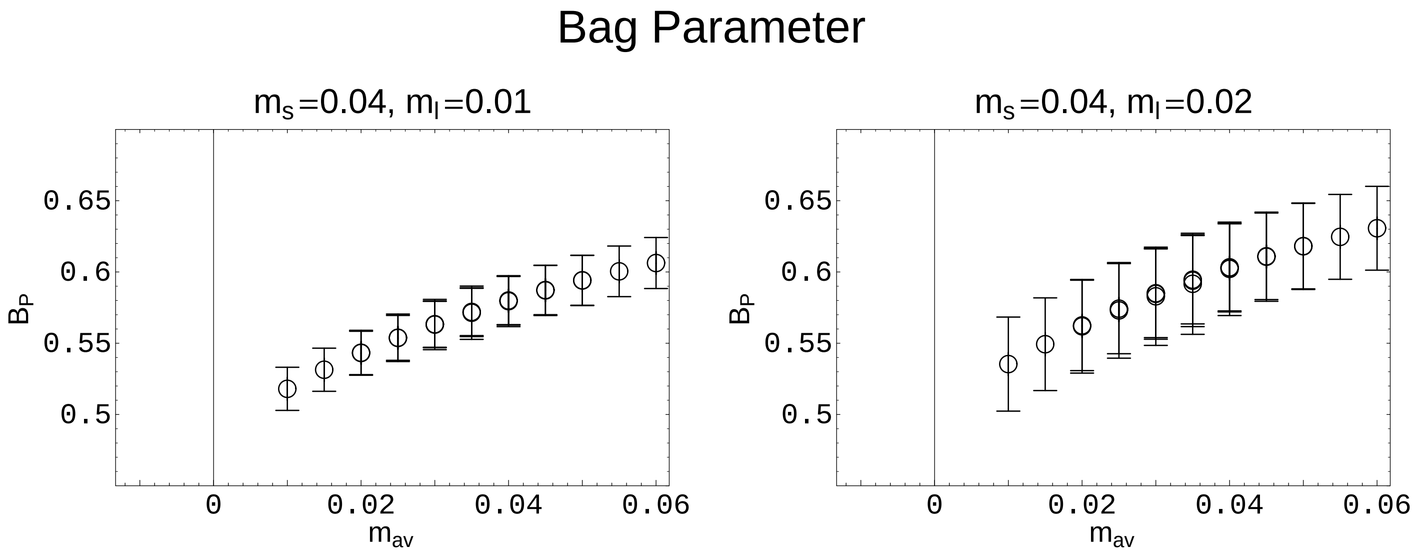

The Bag Parameter

Two Approaches – Clever Approach

$$B_P = \frac{M_P^2 V}{2\frac{8}{3}(m_q + m_{\rm res})^2} \frac{\mathcal{C}_{wpw}^{P\mathcal{O}P}(t_{\rm src}, t, t_{\rm snk})}{\mathcal{C}_{wp}^{PP}(t_{\rm src}, t)\mathcal{C}_{wp}^{PP}(t, t_{\rm snk})}$$

Bag Parameter

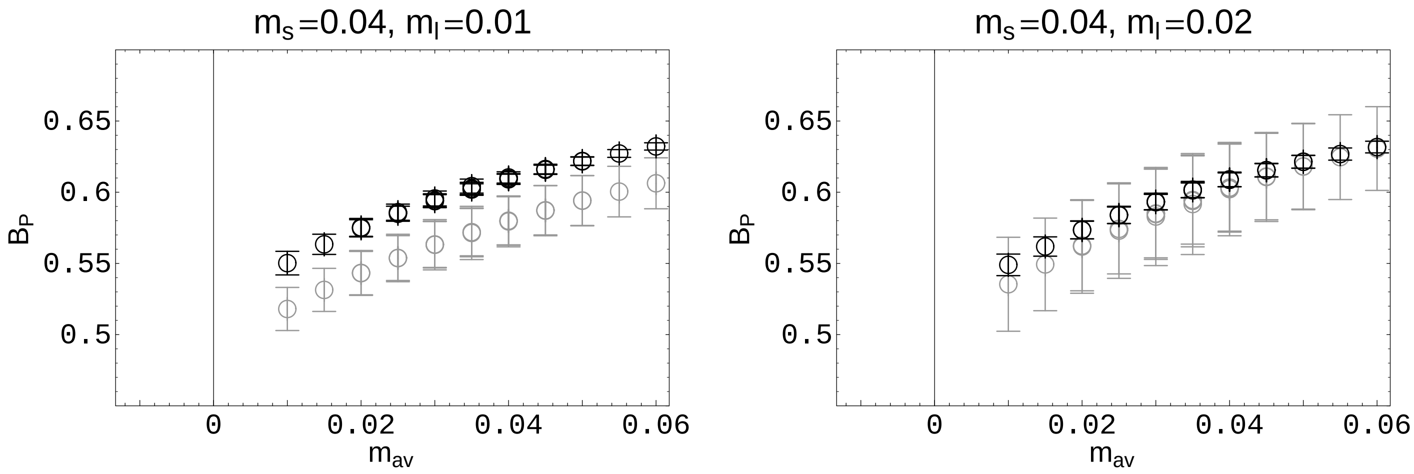

The Bag Parameter

B_K Chiral Fit

The full B_K is fit to a form including the leading part of the chiral fit to f_P.

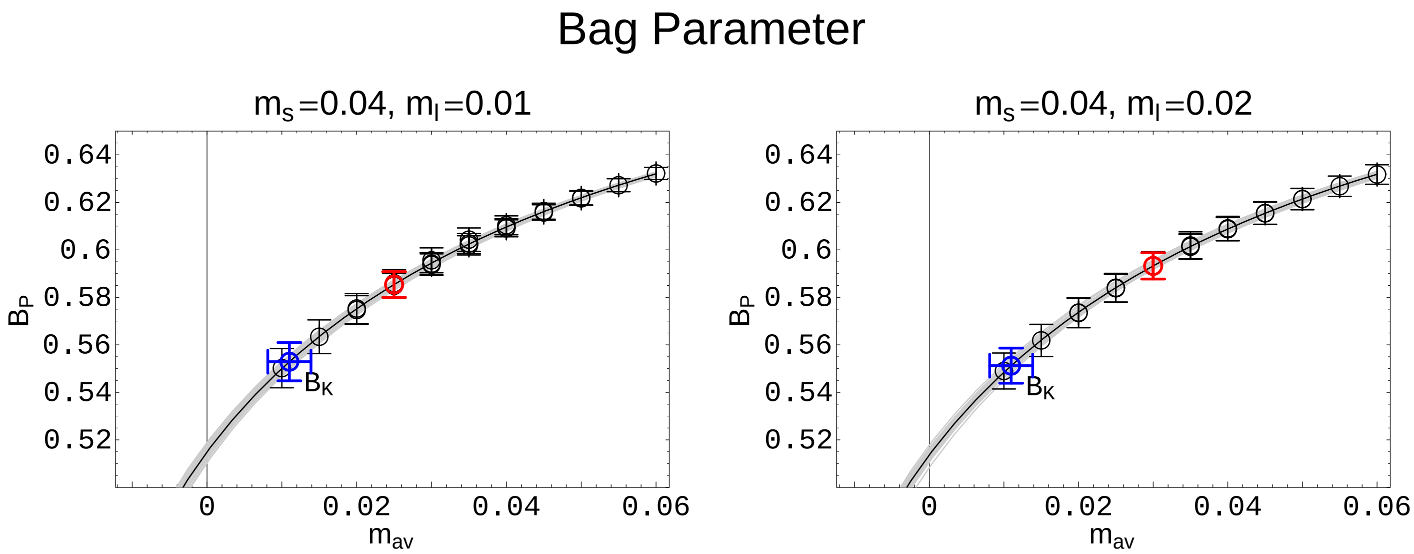

2+1 PQ Chiral Form

Sharpe and van de Water's Chiral Form

For DWF, we may use continuum chiral forms, shifted by the residual mass. From the appendix of (hep-lat/0507012):

$$\left(\frac{B_K}{B_0}\right)^{\text{PQ, 2+1}} = 1+\frac{1}{48\pi^2 f^2 m_{xy}^2}\left[I_{conn}+I_{disc}+bm_{xy}^4+c(m_X^2-m_Y^2)^2+dm_{xy}^2(2m_D^2+m_S^2)\right]$$

2+1 PQ Chiral Form

Sharpe and van de Water's Chiral Form

For DWF, we may use continuum chiral forms, shifted by the residual mass. From the appendix of (hep-lat/0507012):

$$\left(\frac{B_K}{B_0}\right)^{\text{PQ, 2+1}} = 1 + \frac{1}{48\pi^2 f^2 m_{xy}^2}\left[I_{conn} + I_{disc} + b m_{xy}^4 + c(m_X^2 - m_Y^2)^2 + d m_{xy}^2 (2m_D^2 + m_S^2)\right]$$

$$\begin{aligned} I_{conn} &= 6m_{xy}^4 \tilde{\ell}(m_{xy}^2) - 3\ell(m_X^2)(m_{xy}^2 + m_X^2) - 3\ell(m_Y^2)(m_{xy}^2 + m_Y^2) \\ I_{disc} &= I_X + I_Y + I_\eta \end{aligned}$$

$$\begin{aligned} \int \frac{d^4q}{(2\pi)^4} \frac{1}{q^2 + m^2} &\equiv \frac{1}{16\pi^2}\ell(m^2) \\ \int \frac{d^4q}{(2\pi)^4} \frac{1}{(q^2 + m^2)^2} &\equiv \frac{1}{16\pi^2}\tilde{\ell}(m^2) \end{aligned}$$

2+1 PQ Chiral Form

Sharpe and van de Water's Chiral Form

For DWF, we may use continuum chiral forms, shifted by the residual mass. From the appendix of (hep-lat/0507012):

$$\left(\frac{B_K}{B_0}\right)^{\text{PQ, 2+1}} = 1+\frac{1}{48\pi^2 f^2 m_{xy}^2}\left[I_{conn}+I_{disc}+bm_{xy}^4+c(m_X^2-m_Y^2)^2+dm_{xy}^2(2m_D^2+m_S^2)\right]$$

$$\begin{aligned} I_X \quad = \quad & \tilde{\ell}(m_X^2)\frac{(m_{xy}^2+m_X^2)(m_D^2-m_X^2)(m_S^2-m_X^2)}{(m_\eta^2-m_X^2)} \\ - \quad & \ell(m_X^2)\left[\frac{(m_{xy}^2+m_X^2)(m_D^2-m_X^2)(m_S^2-m_X^2)}{(m_\eta^2-m_X^2)^2}\right. \\ + \quad & \frac{2(m_{xy}^2+m_X^2)(m_D^2-m_X^2)(m_S^2-m_X^2)}{(m_Y^2-m_X^2)(m_\eta^2-m_X^2)} \\ + \quad & \left.\frac{(m_D^2-m_X^2)(m_S^2-m_X^2)-(m_{xy}^2+m_X^2)(m_S^2-m_X^2)-(m_{xy}^2+m_X^2)(m_D^2-m_X^2)}{(m_\eta^2-m_X^2)}\right] \end{aligned}$$

2+1 PQ Chiral Form

Sharpe and van de Water's Chiral Form

For DWF, we may use continuum chiral forms, shifted by the residual mass. From the appendix of (hep-lat/0507012):

$$\left(\frac{B_K}{B_0}\right)^{\text{PQ, 2+1}} = 1+\frac{1}{48\pi^2 f^2 m_{xy}^2}\left[I_{conn}+I_{disc}+bm_{xy}^4+c(m_X^2-m_Y^2)^2+dm_{xy}^2(2m_D^2+m_S^2)\right]$$

$$\begin{aligned} I_Y &= I_X(X \leftrightarrow Y) \\ I_\eta &= \ell(m_\eta^2)\frac{(m_X^2-m_Y^2)^2(m_{xy}^2+m_\eta^2)(m_D^2-m_\eta^2)(m_S^2-m_\eta^2)}{(m_X^2-m_\eta^2)^2(m_Y^2-m_\eta^2)^2} \end{aligned}$$

2+1 PQ Chiral Form

B_K Chiral Fit

Now B_K is fit to the 2+1 partially quenched chiral form. Colored bands indicate different valence strange quark masses. Valence light quark mass runs along the x-axis.

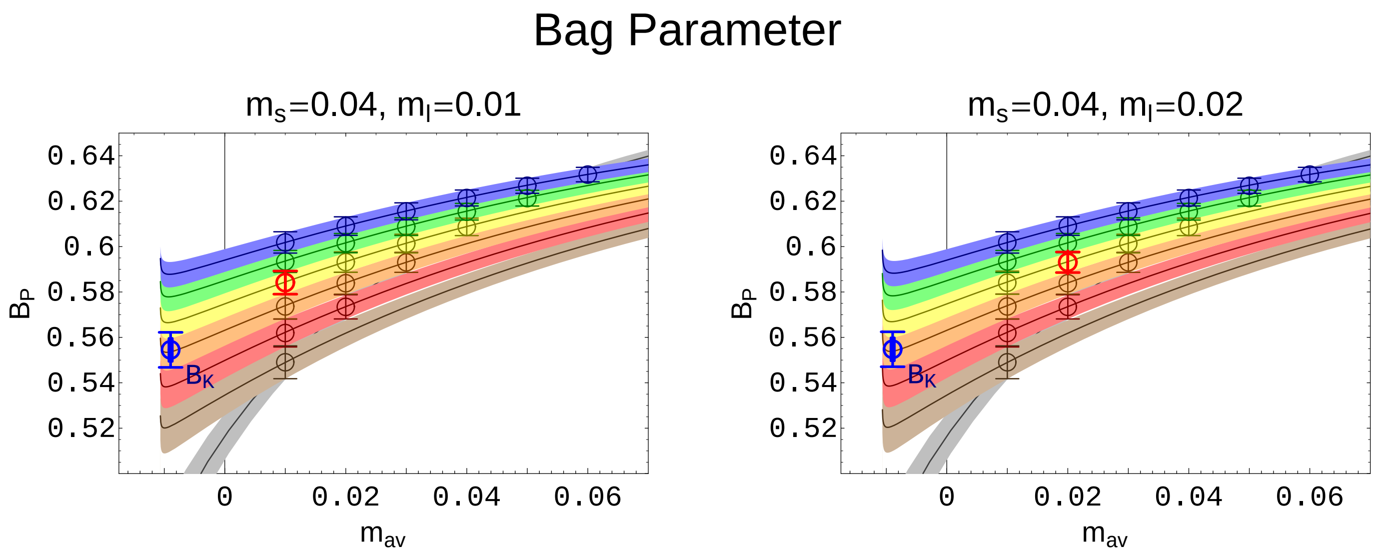

2+1 PQ Chiral Form

B_K Chiral Fit

The new fit is still consistent with the degenerate form. Now average valence quark mass runs along the x-axis. The physical value of B_K is shifted slightly higher.

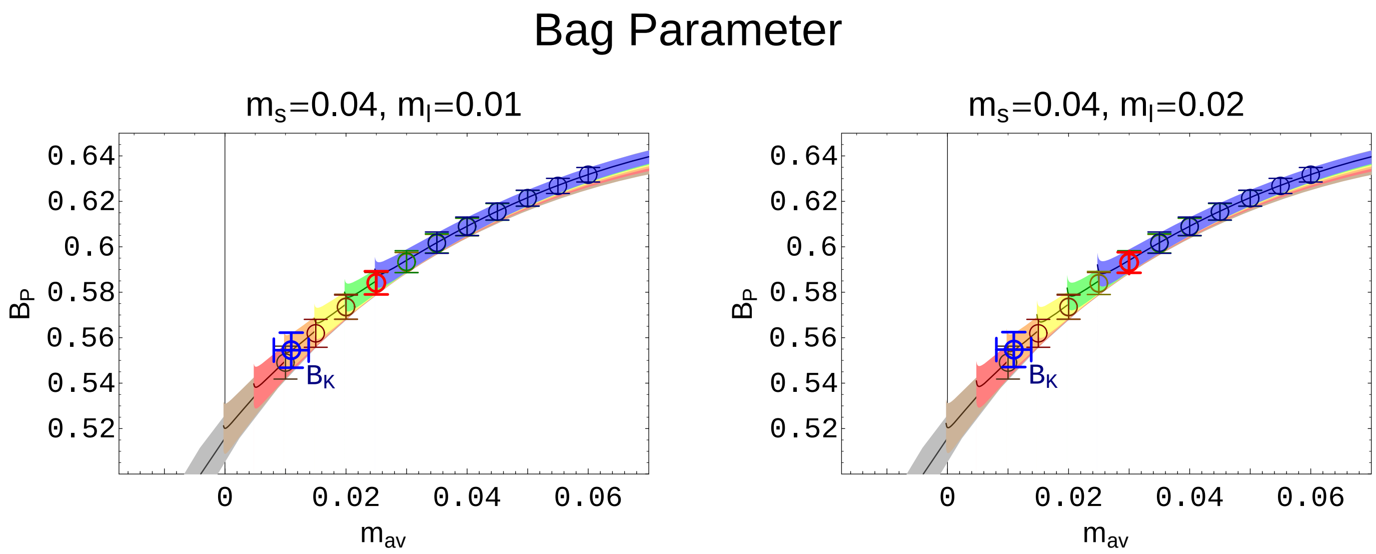

2+1 PQ Chiral Form

Dynamical Extrapolations

Taking the valence=sea point (red) for each set of lattices, we may extrapolate both to the physical limit for the light quarks.

Or taking the valence=physical point (blue) for each set of lattices, we may extrapolate just the light sea quarks by themselves to the physical point.

Bag Parameter

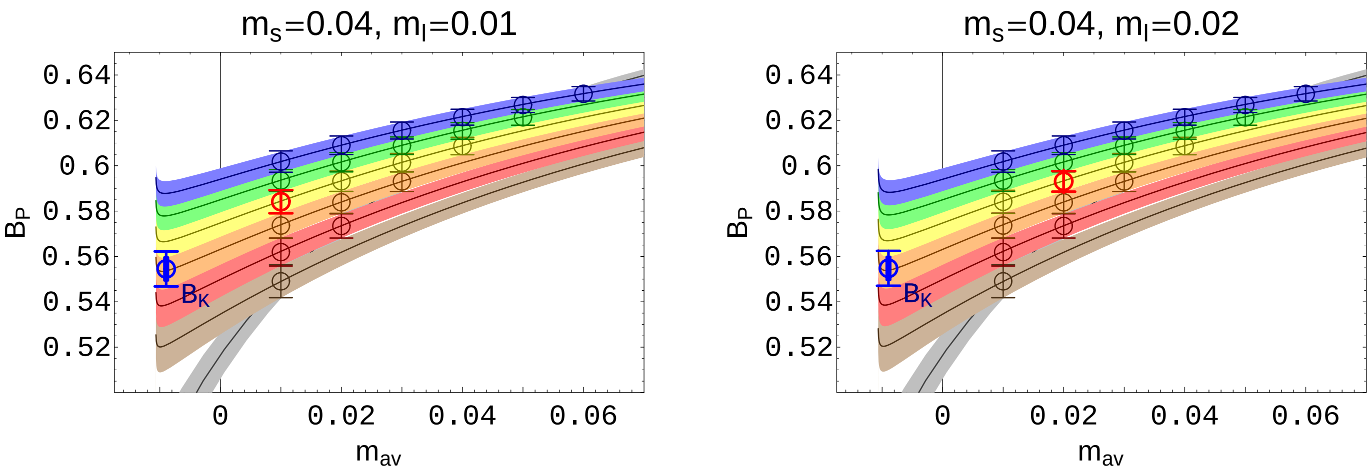

2+1 PQ Chiral Form

Dynamical Extrapolations

Taking the valence=sea point (red) for each set of lattices, we may extrapolate both to the physical limit for the light quarks.

Or taking the valence=physical point (blue) for each set of lattices, we may extrapolate just the light sea quarks by themselves to the physical point.

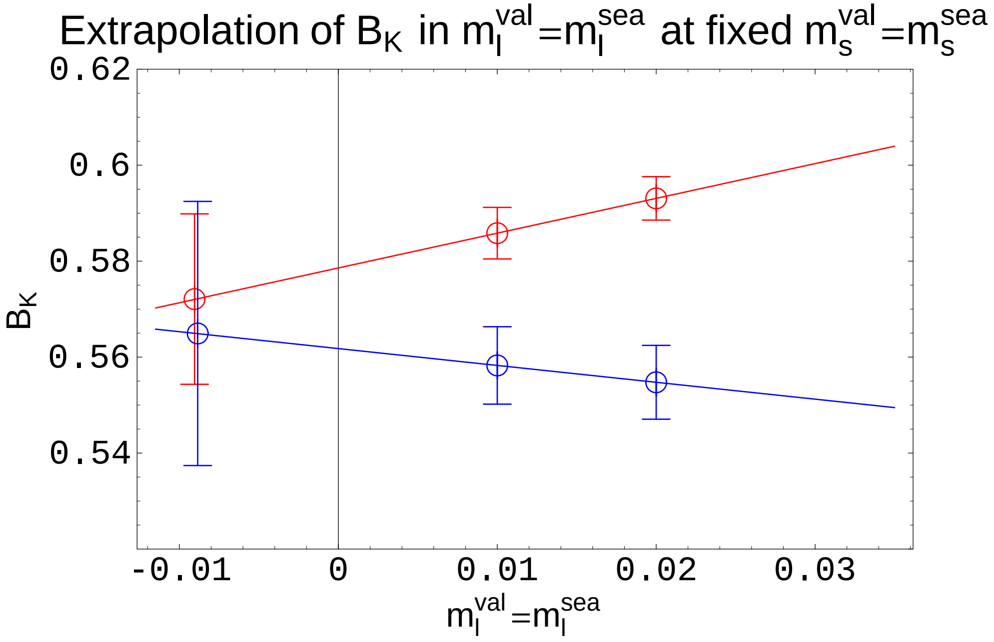

B_K= 0.567(17)

B_K= 0.554(27)

Convolved Source

Convolved Random Box Source

On larger lattices, wall source is too large to overlap with realistic meson states. Box sources induce higher-momentum states. Convolved box source projects to zero momentum.

$$s(\vec{x}) = \sum_{|\vec{x}-\vec{y}|<L_{\mathrm{box}}} \eta(y)$$

The source is translationally invariant in space, so does not induce higher momentum states. The fluctuation of the noisy sources cancel outside the size of the box, so we should see good overlap with realistic mesons.

Convolved Source

Pseudoscalar Plateau

The convolved source on a 24^3 volume shows excellent agreement with the wall source on 16^3.

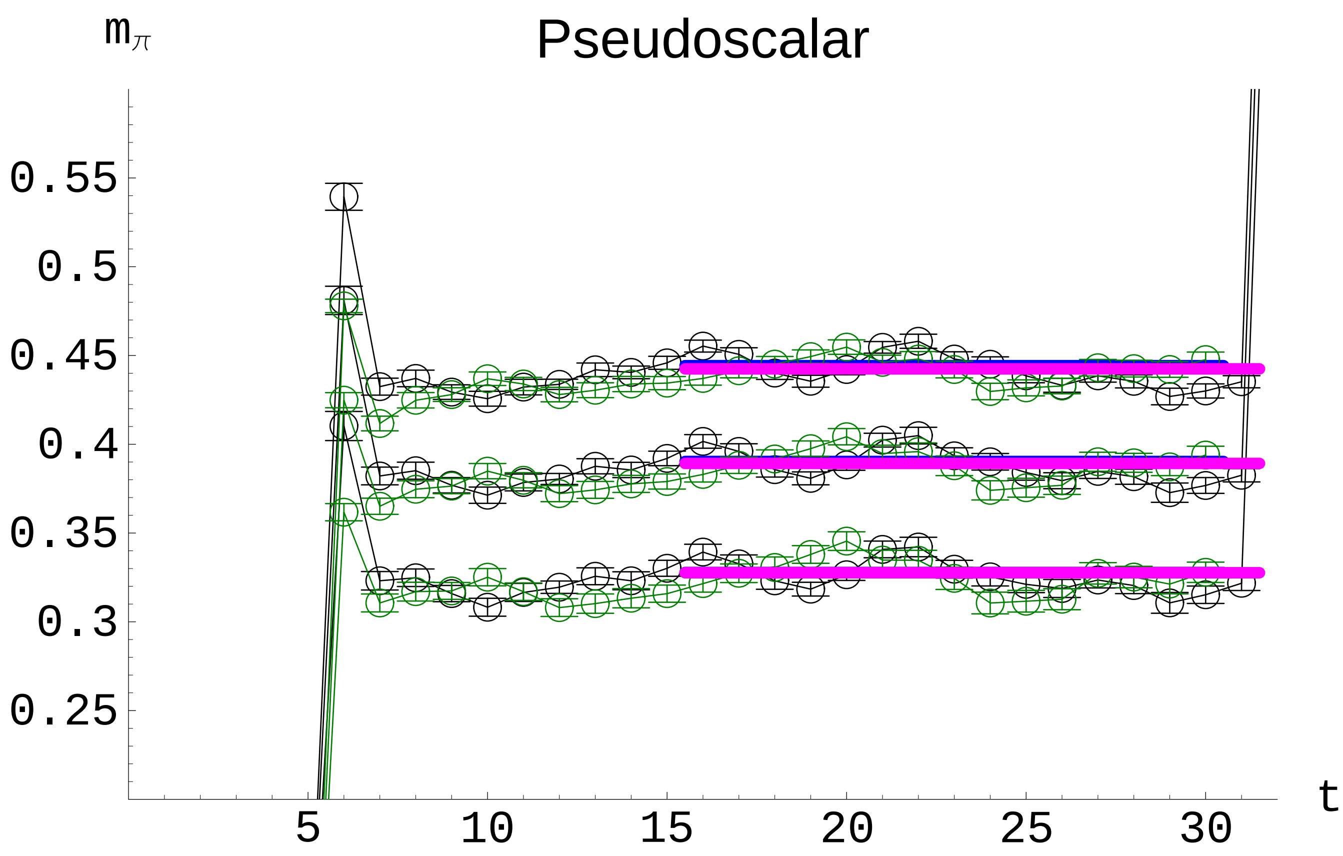

Convolved Source

Wall-Wall Pseudoscalar Plateau

The fluctuations of the wall-wall pseudoscalar are less encouraging.

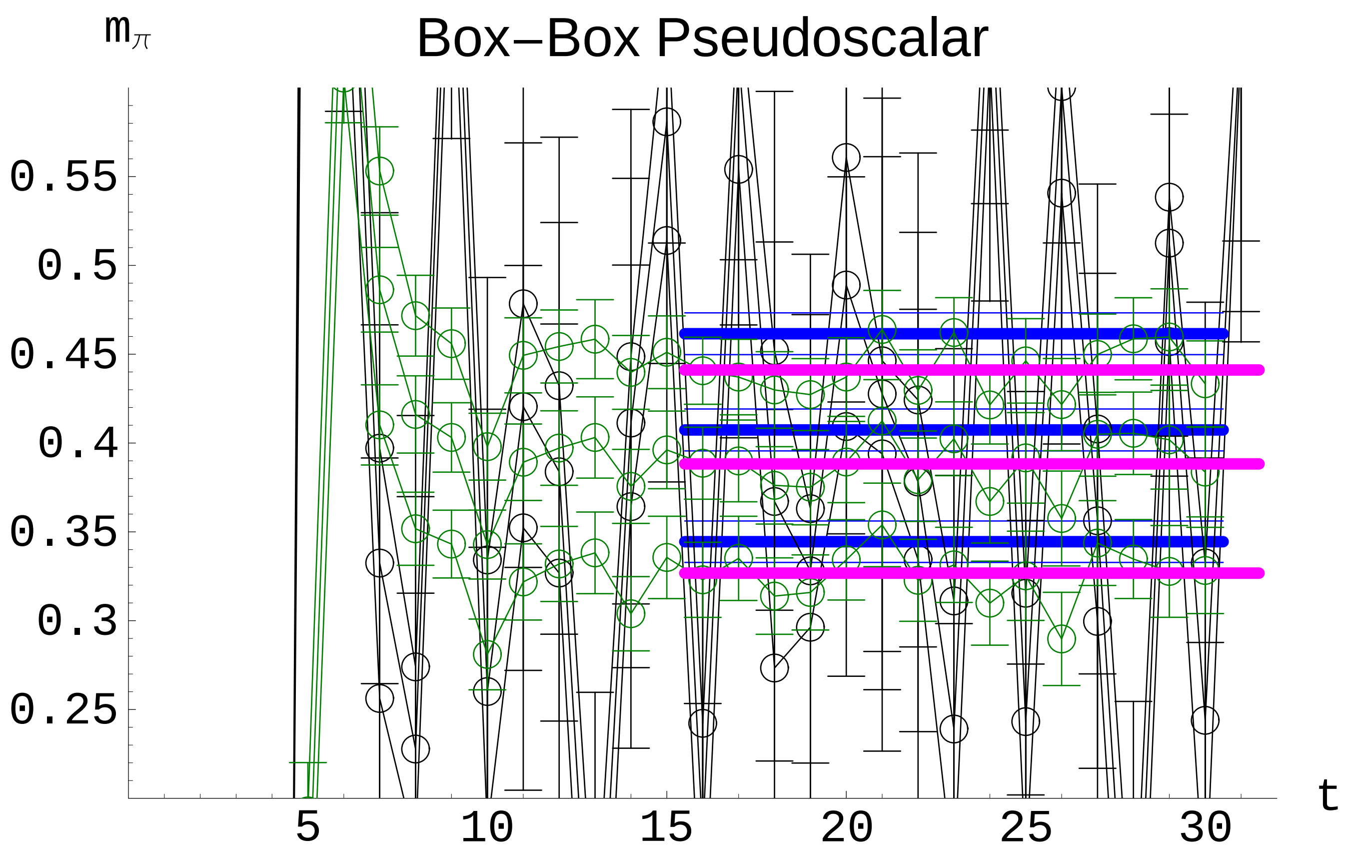

Convolved source

Kaon Bag Parameter

However, at least one of our methods for determining the kaon bag parameter does not require the wall-point correlator.

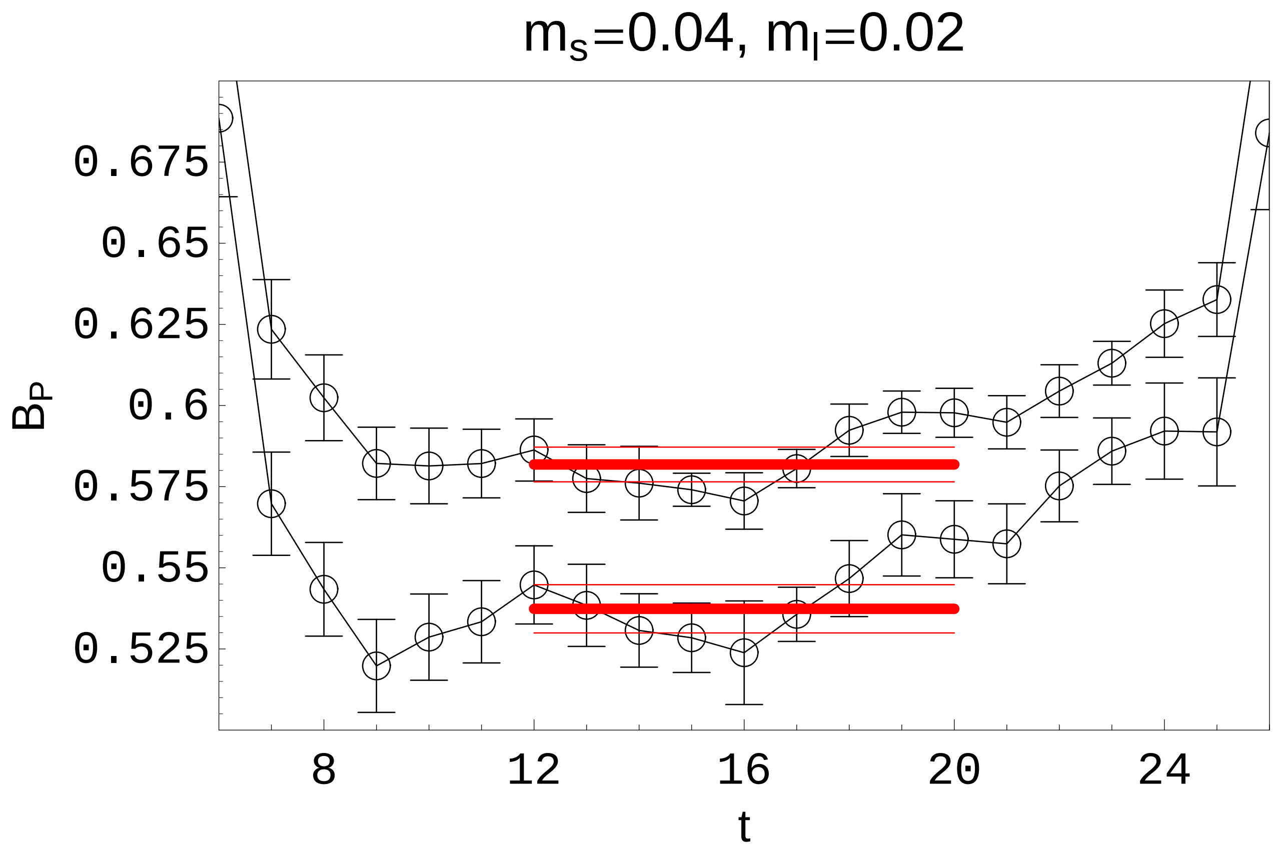

Convolved source

Kaon Bag Parameter

However, at least one of our methods for determining the kaon bag parameter does not require the wall-point correlator.

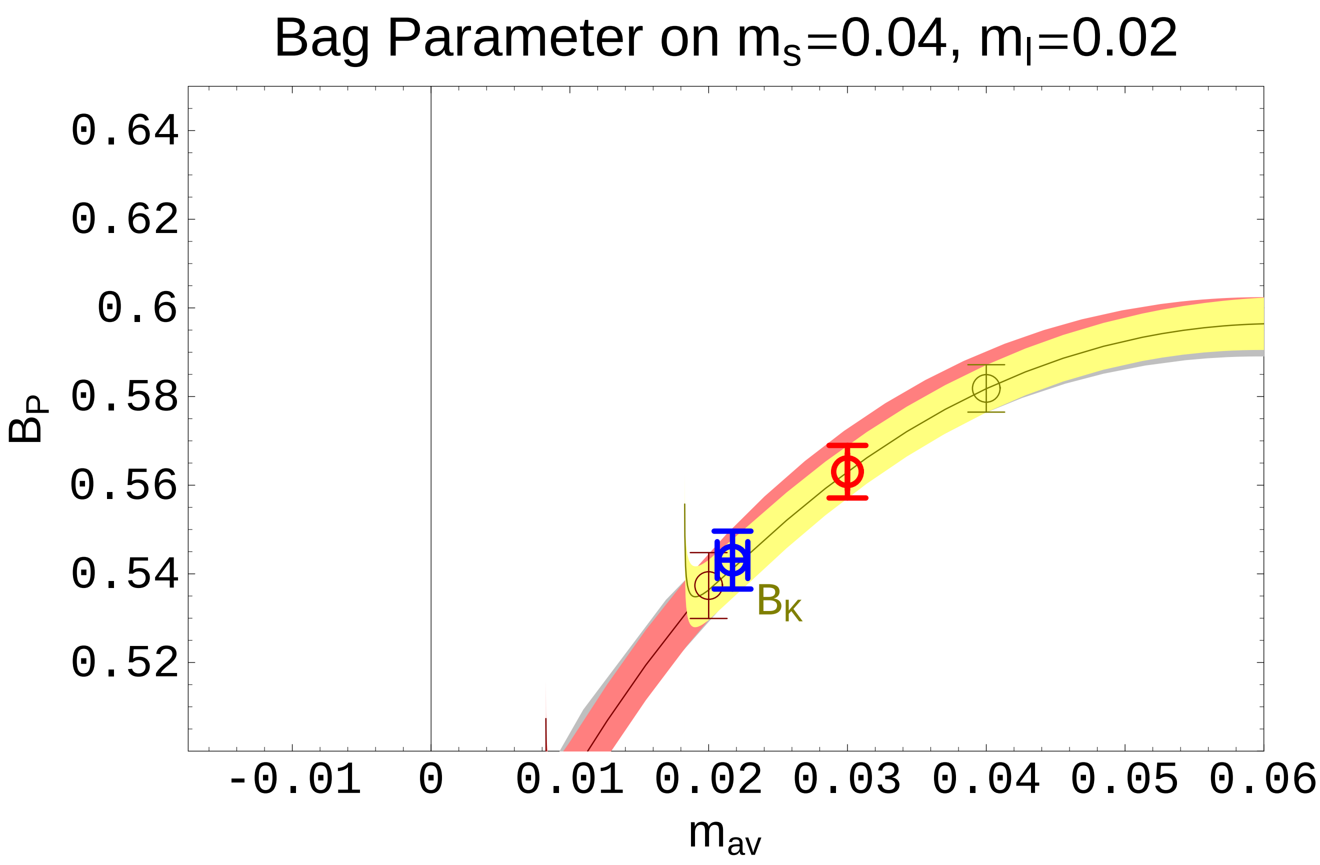

Summary

$24^3 \times 64$ Production Run

– Tuning parameters has yielded increased speed

– Runs are thermalized and continue to progress

– Measurements are beginning to be made on these lattices

B_K Technology

– Proper 2+1 partially quenched chiral form slightly increases B_K

– Larger volumes call for new sources, but may not be practical for other $\Delta S = 1$ operators